ANALYSIS OF PLASMA WAVE INTERFERENCE PATTERNS

IN THE SPACELAB 2 PDP DATA

by

Wei Feng

An Abstract

Of a thesis submitted in partial fulfillment
of the requirements for the Doctor of
Philosophy degree in Physics
in the Graduate College of
The University of Iowa

December 1992

Thesis supervisors: Professor Donald A. Gurnett

ABSTRACT

During the Spacelab 2 mission the University of Iowa's Plasma Diagnostics Package (PDP) explored the plasma environment around the shuttle. Wideband spectrograms of plasma waves were obtained from the PDP at frequencies from 0 to 30 kHz and at distances up to 400 m from the shuttle. These spectrograms frequently showed interference patterns caused by waves with wavelengths short compared to the antenna length (3.89 meters). Two types of interference patterns were observed in the wideband data: the first type was associated with the ejection of an electron beam from the space shuttle; the second type was associated with lower hybrid waves generated by an interaction between the neutral gas cloud around shuttle and the ambient ionospheric plasma. Analysis of these antenna interference patterns permits a determination of the wavelength, the plasma rest frame frequency, the direction of propagation, the power spectrum and in some cases the location of the source.

The electric field noise associated with the electron beam was observed in the wideband data for two periods during which an electron beam was being ejected from the shuttle. This noise always has a broad frequency range at low frequencies (below 10 kHz) and shows clear evidence of interference patterns. The broadband low frequency noise was the dominant type of noise produced by the electron beam. Analysis of the interference patterns produced by this noise shows that the waves

have a linear dispersion relation very similar to ion acoustic waves. The waves are believed to be generated by the current of ambient electrons returning to the shuttle in response to the ejected electron beam. The waves associated with the lower hybrid resonance have rest frame frequencies near the lower hybrid frequency and propagate perpendicular to the magnetic field. The occurrence of these waves depends strongly on the PDP's position relative to the shuttle and the magnetic field direction. Our results confirm previous identifications of these waves as lower hybrid waves and suggest they are driven by pick-up ions (H_2O^+) produced by a charge exchange interaction between a water cloud around the shuttle and the ambient ionosphere.

Abstract approved: _David A. Gurnett_

Thesis supervisor

Prof., Physics and Astronomy

Title and department

Dec 17, 1992

Date

ANALYSIS OF PLASMA WAVE INTERFERENCE PATTERNS

IN THE SPACELAB 2 PDP DATA

by

Wei Feng

A thesis submitted in partial fulfillment
of the requirements for the Doctor
of Philosophy degree in Physics
in the Graduate College of
The University of Iowa

December 1992

Thesis supervisors: Professor Donald A. Gurnett

Graduate College
The University of Iowa
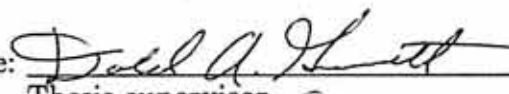Iowa City, Iowa

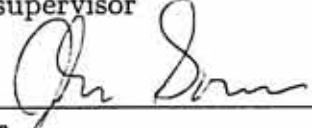CERTIFICATE OF APPROVAL

_____

PH.D. THESIS

_____

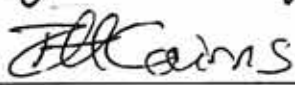This is to certify that the Ph.D. thesis of

Wei Feng

has been approved by the Examining Committee
for the thesis requirement for the Doctor of
Philosophy degree in Physics at the December 1992
graduation.

Thesis committee: _____
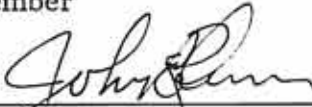   Thesis supervisor

                  _____
                  Member

                  _____
                  Member

                  _____
                  Member

                  _____
                  Member

ACKNOWLEDGMENTS

ABSTRACT

During the Spacelab 2 mission the University of Iowa's Plasma Diagnostics
Package (PDP) explored the plasma environment around the shuttle. Wideband
spectrograms of plasma waves were obtained from the PDP at frequencies from
0 to 30 kHz and at distances up to 400 m from the shuttle. These spectrograms
frequently showed interference patterns caused by waves with wavelengths short
compared to the antenna length (3.89 meters). Two types of interference patterns
were observed in the wideband data: the first type was associated with the ejection
of an electron beam from the space shuttle; the second type was associated with
lower hybrid waves generated by an interaction between the neutral gas cloud
around shuttle and the ambient ionospheric plasma. Analysis of these antenna
interference patterns permits a determination of the wavelength, the plasma rest
frame frequency, the direction of propagation, the power spectrum and in some
cases the location of the source.

The electric field noise associated with the electron beam was observed in
the wideband data for two periods during which an electron beam was being ejected
from the shuttle. This noise always has a broad frequency range at low frequencies
(below 10 kHz) and shows clear evidence of interference patterns. The broadband
low frequency noise was the dominant type of noise produced by the electron beam.
Analysis of the interference patterns produced by this noise shows that the waves

iii

have a linear dispersion relation very similar to ion acoustic waves. The waves are believed to be generated by the current of ambient electrons returning to the shuttle in response to the ejected electron beam. The waves associated with the lower hybrid resonance have rest frame frequencies near the lower hybrid frequency and propagate perpendicular to the magnetic field. The occurrence of these waves depends strongly on the PDP's position relative to the shuttle and the magnetic field direction. Our results confirm previous identifications of these waves as lower hybrid waves and suggest they are driven by pick-up ions (H_2O^+) produced by a charge exchange interaction between a water cloud around the shuttle and the ambient ionosphere.

TABLE OF CONTENTS

LIST OF TABLES

LIST OF SYMBOLS

Symbol	Definition
α_k	angle between $\mathbf{V}_{sc}$ and $\mathbf{k}_{xz}$
$\mathbf{B}$	magnetic field
$\mathbf{E}$	electric field
$F(\alpha_k)$	wave angular distribution function
κ	Boltzmann's constant
k	wavenumber
$k_\parallel$	wavenumber parallel to magnetic field
$k_\perp$	wavenumber perpendicular to magnetic field
$\mathbf{k}$	wavevector
K_i	dielectric constant
l	antenna length
m	null number in interference pattern
m_{O^+}	oxygen ion mass
m_e	electron mass
n_b	beam electron density
n_e	ambient electron density
n_{O^+}	oxygen ion density
R_i	oxygen ion gyroradius

Symbol	Definition
$\Delta\Theta$	beam-arc distribution angle
Ω_{ce}	electron cyclotron frequency
Ω_{ci}	oxygen ion cyclotron frequency
ω_{pe}	electron plasma frequency
ω_{pi}	oxygen ion plasma frequency
ω_0	frequency in plasma rest frame
ω'	frequency in the shuttle frame
ω_{LHR}	lower hybrid frequency
T_e	electron temperature
T_{H_2O+}	water ion temperature
T_{O+}	oxygen ion temperature
V_b	electron beam drift speed
V_e	return electron drift speed
V_{te}	electron thermal speed
V_{ti}	oxygen ion thermal speed
$\mathbf{V_g}$	group velocity
V_s	phase speed
$\mathbf{V_{sc}}$	shuttle velocity
γ	growth rate
λ	wavelength

CHAPTER I

INTRODUCTION

This thesis focuses on wideband interference patterns observed by a plasma
wave receiver carried on a University of Iowa spacecraft called the Plasma Diag-
nostics Package (PDP). The PDP was carried into orbit by the space shuttle as
part of the Spacelab 2 mission. This mission was launched on July 29, 1985, into
a nearly circular low inclination orbit with an altitude of about 320 km and an
inclination of 49.5 degrees. One of the prime objectives of the Spacelab 2 mission
was to explore the plasma environment around the shuttle. During a six-hour free
flight period on August 1, 1985, the PDP was released and completed two fly-
arounds of the shuttle at distances out to 400 meters. To investigate beam-plasma
interactions, a 1-keV electron beam was ejected from the shuttle at certain times
during the mission. To explore these and other phenomena, the PDP carried a
full complement of particle and field instruments. Reviews of the PDP spacecraft,
the instruments, and the observations are given by Shawhan [1982] and Kurth and
Frank [1990].

Basically, the previous work on the PDP plasma observations can be divided
into two groups. The first group was associated with the ejection of the electron
beam from the shuttle, and the second group was associated with the plasma
environment around the shuttle. The plasma wave receiver on the PDP spacecraft

detected intense waves during times when the electron gun was being operated [Gurnett et al., 1986; Farrell et al., 1988; Reeves et al., 1988, 1990]. Gurnett et al. [1986] reported on funnel-shaped whistler mode radiation from electron beams during the 0330–0337 UT magnetic conjunction. The characteristic frequency-time shape of the funnel is a propagation effect that occurs for waves near the resonance cone. Farrell et al. [1988] estimated the total whistler mode power radiated by the electron beam. They concluded that the observed whistler mode radiation is Cerenkov radiation from coherently radiating electron bunches in the beam. Frank et al. [1989] showed measurements of hot electrons during the 0411–0418 UT magnetic conjunction. These measurements identified the existence of a return current associated with the electron beam. The return current exists in the form of a sheet with a thickness of 20 meters that extends 170 meters or more downstream from the shuttle. Large intensifications of the broadband waves were observed in association with the returning electrons, especially at very low frequencies. Reeves et al. [1988] reported on broadband, very low frequency (VLF) electromagnetic wave emissions from both steady state (DC) electron beams and modulated electron beams during magnetic conjunctions. The modulated electron beams produced narrowband emissions at both the fundamental and its harmonics. Reeves et al. [1990] compared the narrowband radiation with coherent radiation theory and showed that both coherent and incoherent processes are involved in producing the narrowband radiation. All the above papers concentrated on the data from electron beam firings during the two magnetic conjunction events at 0330–0337 UT and 0411–0418 UT. Feng et al. [1992a] analysed the interference

patterns in the wideband data. The very low frequency (up to a few hundred Hz in the ambient plasma rest frame) emissions associated with the electron beam were identified as oblique ion acoustic-like waves.

Intense plasma wave turbulence was also observed by the PDP's plasma wave receiver and Langmuir probe even when the electron beam was not operating [Gurnett et al., 1988; Pickett et al., 1989; Cairns and Gurnett, 1991a,b]. This turbulence occurred primarily downstream of the shuttle and along magnetic field lines passing near the shuttle. The intensities also tended to increase during times of frequent thruster firings. Langmuir probe data have also been used to investigate low frequency waves (below about 40 Hz) associated with water dumps and the shuttle's orbital maneuvering system and plasma wake [Murphy et al., 1989; Pickett et al., 1989; Tribble et al., 1989]. Paterson and Frank [1989] showed that the shuttle is surrounded by an energized distribution of H_2O^+ ions. These ions are believed to be produced by a charge exchange interaction between a water cloud outgassing from the shuttle and ambient ionospheric O^+ ions. Cairns and Gurnett [1991a] showed that the amplitude and spectral character of the plasma waves observed by the free-flying PDP is controlled by the angle between the magnetic field and the velocity of the shuttle relative to the ionospheric plasma. Large wave amplitudes and a characteristic "mushroom-shaped" frequency-time structure were observed in the broadband electric field spectrum when the velocity vector was nearly perpendicular to the magnetic field. A band of noise near the top of the mushroom was identified with the lower hybrid frequency. The base of the "mushroom" consisted of a triangular-shaped emission that started at low

frequencies and extended up to the lower hybrid frequency near the center of the "mushroom". Cairns and Gurnett [1991a] interpreted the base of the "mushroom" as Doppler-shifted lower hybrid waves driven by water ions produced by the charge exchange process. They suggested that the waves are generated both locally and in the vicinity of the shuttle. The shuttle-associated waves observed in the near zone have been characterized and interpreted in detail by Cairns and Gurnett [1991b], again in terms of Doppler-shifted lower hybrid waves. The near zone is defined as the region within 10 meters of the shuttle. The source of the waves is believed to be a beam-arc distribution of water ions formed in the vicinity of the shuttle. Based on this idea, Rivas and Hastings [1992] have done further work on the near zone waves. They interpreted both peaks in the observed wave spectrum in terms of lower hybrid waves, with the peaks corresponding to waves propagating in different directions. Feng et al. [1992b] identified the Doppler-shifted lower hybrid waves in the wideband data.

This thesis presents a detailed analysis of so-called "fingerprint" patterns in the electrostatic wave spectra from the PDP wideband receiver [Feng et al., 1992a,b]. "Fingerprint" patterns are well known in space plasma physics. They are spin-modulated antenna interference patterns caused by electrostatic waves with wavelengths short compared to the antenna length [Temerin, 1979; Fuselier and Gurnett, 1984; Gallagher, 1985]. Antenna interference patterns are frequently observed in the wideband data when the PDP is downstream from the shuttle. Two types of interference patterns are observed: one corresponding to waves at very low frequencies (below a few hundreds Hz) [Feng et al., 1992a]; and the

other corresponding to lower hybrid waves [Feng et al., 1992b]. The low frequency waves were produced by the electron beam ejected by the shuttle, and the lower hybrid waves were produced by charge exchange ions. A brief description of the Spacelab 2 mission and the PDP are given in Chapter II. A theoretical review of antenna interference effects is presented in Chapter III. The observational data are presented in Chapter IV. The analysis of the first type of interference pattern is conducted in Chapter V. This analysis shows that the low frequency waves are obliquely propagating ion acoustic-like waves. The results from a linear growth rate analysis of ion acoustic-like instabilities are presented and compared with observation. The analysis of the second type of interference pattern is conducted in Chapter VI. This analysis shows that the lower hybrid waves are propagating at wave normal angles nearly perpendicular to the static magnetic field. A strong case is presented that these waves are produced by pick-up ions from the shuttle water cloud. Finally, the conclusions of the thesis are given in Chapter VII.

CHAPTER II

DESCRIPTION OF THE SPACELAB 2 MISSION AND THE PDP

Spacelab 2 was launched into a nearly circular low-inclination orbit with a nominal altitude of about 320 km and an inclination of 49.5°. During the flight the Plasma Diagnostics Package (PDP) was released from the space shuttle to investigate phenomena associated with the passage of a large vehicle through the ionosphere and the injection of electron beams into the ambient ionosphere. The PDP provided observations in free flight out to a distance of about 400 m from the shuttle. A Langmuir probe, an ion mass spectrometer, a hot plasma analyzer, a differential ion flux probe, and a plasma wave receiver were among the instruments on board the PDP. The PDP was designed and constructed at the University of Iowa and was a reflight of the spacecraft previously flown on the STS-3 flight [Shawhan at al., 1984]. The PDP spacecraft carried a full complement of particle and field instruments. A two-dimensional view of the PDP and sketch showing the location of the instruments around the perimeter of the spacecraft are shown in Figure 2.1.

The PDP was in free flight around the shuttle from 0010 to 0620 UT on August 1, 1985. Plasma parameters during the free flight are given in Table 2.1. During this roughly 6-hour interval, the shuttle performed two complete fly-arounds of the PDP. These fly-arounds provided measurements both upstream

and downstream from the shuttle, and along the magnetic field lines threading the shuttle. In addition to the fly-arounds, a series of wake transits were performed to survey the wake region directly downstream from the shuttle. Among the various investigations performed was one to study the effects produced by a 1-keV electron beam ejected from the shuttle, the so-called Fast Pulse Electron Generator (FPEG) experiment [Shawhan, 1982; Bash et al., 1987; Reeves et al., 1988, 1990]. The electron beam was operated during two magnetic conjunctions between the shuttle and the PDP (0330–0337 UT and 0411–0418 UT), and also at other times (0046–0050 UT, 0119–0123 UT and 0247–0250 UT) when the PDP was not magnetically connected to the shuttle. The FPEG generated a 1-keV electron beam at currents of either 50 mA or 100 mA and had the capability of operating in a pulsed or direct current (DC) mode. In the pulsed mode of operation the electron beam could be modulated over a wide range of pulse periods, duty cycles and number of pulses. A variety of sequences were executed in order to perform quantitative investigations of electromagnetic radiation and associated plasma disturbances from both DC and pulsed electron beams. Artificially generated electron beams such as the FPEG experiment provide a unique means to investigate beam-plasma interactions under relatively controlled conditions. Motivations for such injection experiments include the simulation of natural auroral phenomena and vehicle charging effects [Winckler, 1980; Bush, 1987], as well as the generation of plasma waves.

During the six hours of free flight, the PDP was spin stabilized with a rotation period of about 13.6 seconds. In addition to the wideband receiver, the PDP plasma wave instrument includes an array of band-pass filters. The filter

array included the IMP receiver and the Helios receiver, both of which consisted of a 16 channel spectrum analyzer with 10% bandwidths covering the frequency range from 31 Hz to 178 kHz, and the Medium Frequency Receiver (MFR) which consists of 8 channels with 10% bandwidths in the frequency range 316 kHz to 17.8 MHz. The wideband receiver provides measurement in four frequency bands, with frequency limits of 40 Hz - 1 kHz, 400 Hz - 10 kHz, 10 KHz - 20 kHz, and 20 kHz - 30 kHz. The wideband receiver was connected alternately to the 3.89 meter double sphere electric antenna and to a 16 inch long, 10,000 turn magnetic field search coil. Every fourth magnetic antenna period was replaced by a Langmuir probe period. This antenna switching pattern is shown in Figure 2.2. In addition, the upper three frequency bands are subjected to another switching pattern. In both the electric and magnetic antenna periods, the 0–10 kHz band is measured for 25.6 seconds, and the 20–10 kHz (with inverted frequency response) and the 20–30 kHz bands are measured for 12.8 seconds each, to give a total cycle period of 51.2 seconds. The antenna switching pattern and the band switching pattern account for many of the apparent gaps or discontinuities in the wave data as well as the lack of simultaneous electric and magnetic field data. For the wideband data, the total output signal strength was kept within strict limits by an automatic gain control (AGC). Absolute intensities cannot be obtained directly from the wideband data, and must be computed from the 16 channel spectrum analyzer data.

CHAPTER III

ANTENNA INTERFERENCE EFFECTS

"Fingerprint" patterns in frequency-time spectrograms of plasma wave data are a well-known space plasma wave phenomena. They are caused by electrostatic waves with wavelengths short compared to the antenna [Temerin, 1979; Fuselier and Gurnett, 1984; Gallagher, 1985; Feng et al., 1992a,b]. Typically a periodic pattern of constructive and destructive interference is produced by the spin related rotation of the antenna in the wave field. For fingerprint patterns to be observed, two conditions must be met: (1) the Doppler shift of the waves has to be quite large compared to the rest frame wave frequency, and (2) waves with the same wavenumber must propagate in almost the same direction. The frequency-time spectrum in the wideband data can be then regarded as the wavenumber (or wavelength) - time spectrum. Interference patterns can be used to determine the wavelength, the direction of propagation, the Doppler shift, the rest frame frequency, the angular distribution, and the power spectrum of the waves. An example of an interference pattern observed in the PDP data is shown in the Figure 3.1. This spectrogram was obtained over a 13-second interval (0046:50–0047:13 UT) on August 1, 1985. The "fingerprint" interference pattern caused by the rotation of the antenna in the wave field is clearly evident.

To help understand these interference effects, it is useful to review the response of an electric dipole antenna to an electrostatic wave. The following development is similar to the theory introduced by Temerin [1979] and Gallagher et al. [1985]. The coordinate system used in this study is called the Local Vertical/Local Horizontal (LVLH) reference system. The z-axis in this reference system lies along the geocentric radius vector to the spacecraft and is positive toward the center of the Earth. The x-axis lies in the orbital plane and is positive in the direction of spacecraft motion. The y-axis is normal to the orbital plane and completes the right-handed orthogonal system. The relevant geometry for this coordinate system is illustrated in Figure 3.2. The potential $\triangle \Phi$ of an electrostatic wave between two points in space separated by a vector $d\mathbf{r}$ is given by:

$$\triangle \Phi = -\mathbf{E} \cdot d\mathbf{r}, \tag{1}$$

where $\mathbf{E}$ is the electric field. During the free flight the spin axis of the PDP was oriented perpendicular to the orbital plane. Therefore, we can assume that the electric antenna is rotating in the X-Z plane. The electric field is then given by:

$$\mathbf{E} = (E_{xz}\hat{\rho} + E_y\hat{\mathbf{y}})e^{i(\mathbf{k}\cdot\mathbf{r}-\omega t)},$$

where $\hat{\rho}$ is the unit vector in the X-Z plane and E_{xz} is the magnitude of $\mathbf{E}$ projected onto the X-Z plane. The PDP electric field antenna consists of a double-probe antenna with a separation distance l between the spheres of 3.89 meters. We define $\mathbf{l}$ to be the vector along the antenna axis and k_{xz} to be the magnitude of $\mathbf{k}$ projected onto the X-Z plane. Therefore substituting $\mathbf{l}$ for $\mathbf{r}$, we have $d\mathbf{r} = d\mathbf{l}$ and

$\mathbf{k} \cdot \mathbf{r} = k_{xz}l\cos\phi$, where ϕ is the angle between $\hat{\rho}$ and $\mathbf{l}$. Integrating Equation (1) between two probes located at $-l/2$ and $l/2$ gives

$$\Delta\Phi = \frac{-2(E_{xz}\cos\phi)\sin(k_{xz}(l/2)\cos\phi)e^{-\imath\omega t}}{k_{xz}\cos\phi}. \qquad (2)$$

The measured rms voltage, V_m, is the average potential difference (over time t) between the spheres, which is given by

$$V_m = \frac{[\Delta\Phi\Delta\Phi^*]^{1/2}}{\sqrt{2}} = \frac{E_{xz}l}{\sqrt{2}}|\cos\phi||\frac{\sin(x\cos\phi)}{x\cos\phi}| \qquad (3)$$

where

$$x = \frac{k_{xz}l}{2}.$$

For waves with wavelength in the X-Z plane $\lambda_{xz} \gg l$ the $|sin(x\cos\phi)/x\cos\phi|$ term in Equation (3) approaches unity and the usual spin related cosine modulation of the power spectrum is obtained. If $\lambda \sim l$ then the $|sin(x\cos\phi)/x\cos\phi|$ term produces a characteristic spin-modulated interference pattern that can be observed in the wideband data. To understand this term more thoroughly, it is useful to determine the conditions for minima and maxima in the measured voltage. Minima in the measured voltage occur when $sin(x\cos\phi)$ is zero. This condition can be expressed as

$$\frac{k_{xz}l\cos\phi}{2} = m\frac{\pi}{2} \qquad (4)$$

where m is an even number (m = 2, 4, 6, ...). The null indicated by Equation (4) can be used to determine the wavevector components in the antenna spin plane

(X-Z plane). The characteristic shape of a typical interference pattern can be explained by rewriting Equation (4) in the following form

$$l\cos\phi = \frac{m}{2}\lambda \tag{5}$$

where λ is the wavelength projected onto X-Z plane ($k_{xz} = 2\pi/\lambda$). For a fixed antenna position, Equation (5) shows that the condition for a minimum ($V_m = 0$) is met when an integral number of wavelengths is projected onto the antenna.

To analyze the dispersion relation of the waves, it is useful to determine the frequency in the rest frame of the plasma. The rest frame frequency can be obtained by subtracting the Doppler shift from the frequency measured in the spacecraft frame of reference. The relevant equation is

$$\omega' = \omega_0 - \mathbf{k} \cdot \mathbf{V}_{sc} \tag{6}$$

where ω' is the frequency measured in the spacecraft frame of reference, ω_0 is the frequency in the plasma rest frame and $\mathbf{V}_{sc}$ is the velocity of the spacecraft relative to the plasma. Since the spacecraft velocity vector is directed along the x-axis, this equation simplifies to

$$\omega' = \omega_0 - k_x V_{sc} = \omega_0 - k_{xz} V_{sc} \cos \alpha_{k0} \tag{7}$$

where α_{k0} is the angle between the spacecraft velocity vector and wavevector $\mathbf{k}_{xz}$ which is the projection of the wavevector onto the X-Z plane.

A null at a certain frequency in the wideband data corresponds to a projected wavevector $\mathbf{k}_{xz}$ with zero potential between the tips of the antenna. As the

antenna rotates, the angle ϕ between the projected wavevector and the antenna varies. As the angle ϕ approaches $\pm\pi/2$, larger and larger projected wavenumbers are required to meet the null condition. The null therefore moves to higher frequencies as $\phi \to \pm\pi/2$, thereby forming the walls of the U-shape pattern. The pattern repeats every one-half spacecraft rotation. The center of the U-shaped pattern thus gives the direction of the wavevector projected onto the spin plane of the antenna.

The maximum antenna voltage can also be used to determine the direction of the wavevector projected onto the spin plane. Maxima occur when the condition $\tan(x\cos\phi) = (x\cos\phi)$ is met or approximately when

$$\frac{k_{zz}l\cos\phi}{2} = m\frac{\pi}{2}, \tag{8}$$

where m has the values $m = 0, 2.86, 4.92, 6.94,....$ Note that at $m = 0$ the voltage has its largest maximum. In addition, as may be shown using the turning points of Equation (3), the maximum expected at $m \simeq 1$ disappears due to the strength of the $m = 0$ maximum.

It is important to realize that the analysis of the interference pattern does not give any information about the component of the wavevector perpendicular to the spin plane. This information is lost when the dot product $\mathbf{E} \cdot d\mathbf{r}$ is taken to find the potential. This lack of information must be carefully considered when making wavelength estimations and measurements of the propagation direction. Fortunately, for the PDP data the perpendicular component of the wavevector

does not enter into the calculation of the Doppler shift because the spacecraft spin axis is oriented perpendicular to the plasma flow velocity so that $k_y V_{scy} = 0$.

To interpret the wideband spectrum, the measured voltage spectral density must be related to the electric field spectral density of the wave. From the above discussion one can see that the voltage spectral density is given by

$$P(k_{xz}, \phi) = \frac{(V_m)^2}{\Delta f} = \frac{E_0^2(k_{xz})l^2}{2\Delta f} \frac{\sin^2(x \cos \phi)}{x^2}, \tag{9}$$

where E_0 is the electric field strength and Δf is the measurement bandwidth. The frequency ω' of the wideband data is related to the wavenumber k_{xz} through Equation (7). In reality the waves propagate over a certain range of angles, centered at α_{k0}. Integrating over all propagation angles, assuming an angular distribution function $F(\alpha_k)$, the measured spectral density is given by

$$P_{mea}(k_{xz}, \phi) = (\frac{V_m^2}{\Delta f})_{mea} = \frac{E_0^2(k_{xz})l^2}{2\Delta f} \int F(\alpha_k) \frac{\sin^2(x(\alpha_k) \cos(\phi(\alpha_k)))}{x^2(\alpha_k)} d\alpha_k. \tag{10}$$

Equation (10) will be used to calculate a numerical simulation of interference patterns in Section V. The electric field spectral density corrected for the antenna response is then given by

$$\frac{E_0^2(k_{xz})}{\Delta f} = \frac{2P_{mea}(k_{xz})}{l^2 \int F(\alpha_k) \frac{\sin^2(x(\alpha_k) \cos(\phi(\alpha_k)))}{x^2(\alpha_k)} d\alpha_k}. \tag{11}$$

Using Equation (11), the true density spectrum of the waves as a function of wave number k_{xz} (or frequency) can be deduced from the wideband interference patterns.

CHAPTER IV

OBSERVATIONS

The wideband receiver provides measurements in both the ELF (0–1 kHz) range and the VLF (0.4–30 kHz) range. Interference patterns were only observed in the VLF ranges. Two types of interference patterns were observed. The first type corresponds to waves with very low frequencies (a few hundreds Hz) in the plasma rest frame. These interference patterns are all associated with the ejection of an electron beam [Feng et al., 1992a]. The second type corresponds to waves which have frequencies near the lower hybrid frequency in the plasma rest frame. As will be shown the wave vector direction of these waves is almost perpendicular to the magnetic field [Feng et al., 1992b].

Interference Patterns Associated with Beam-Driven Ion Acoustic-like Waves

The electron gun was operated in various modes during the following time periods: 0046–0050 UT, 0119–0123 UT, 0247–0251 UT, 0330–0337 UT, and 0411–0418 UT. Intense low frequency waves accompany each of these electron gun firings and are closely correlated, in all cases, with the times of the gun firings, within the time resolution of the wave instruments (1.6 seconds). Figure 4.1 shows a broadband electric field spectrogram constructed using Helios and MFR multi-channel data for the time periods 0046–0050 UT, 0119–0123 UT, 0247–0251 UT,

and 0411–0419 UT. The electric field spectral density, $E^2/\Delta f$, where Δf is the bandwidth of the filter channel, is color-coded with blue being the least intense and red being the most intense. The white curves labelled F_{ce} and F_{LH} are the electron cyclotron and lower hybrid frequencies, respectively. The intense (red and yellow color) waves below about 5 kHz are associated with the injected FPEG electron beam. A snapshot of the electric field spectrum at 0046–0047 UT is given in Figure 4.2. The intensity of the low frequency waves (below 10 kHz) is on the order of 1-4 orders of magnitude higher than the intensities at higher frequencies. Accordingly, the dominant waves produced by the ejection of an electron beam are low frequency waves. Note that the frequencies were measured in the frame of the PDP. As we will show in the following analysis, the wavelengths are so short ($\sim$ few meters) that the frequency observed in the spacecraft frame of rest is mainly determined by the Doppler shift. In each of the four events shown in Figure 4.1, complete or partial antenna interference patterns are found in the 0–10 kHz electric field wideband data. Although similar intense low frequency waves are visible in the Helios/MFR data for the 0330–0337 UT event (see Plate 1 in Farrell et al. [1988]), no interference patterns were found in the corresponding 0–10 kHz wideband data.

All the antenna interference patterns associated with electron beam related waves were observed in the 0–10 kHz electric field wideband data. No interference patterns were observed in the 10–20 kHz or 20–30 kHz frequency ranges. The absence of interference patterns in the upper two frequency bands is apparently due to the rapid decrease in wave intensity with increasing frequency. During the

0046–0047 UT and 0247–0250 UT events, very clear interference patterns were observed in the 0–10 kHz data. The corresponding spectrograms are shown in Figure 3.1 and Figure 4.3. The antenna interference patterns correspond exactly with periods of operation of the FPEG gun. During the 0046–0047 UT event, the electron gun was operated in the DC mode from 0046:11 UT to 0047:05 UT. Wideband electric field data in the 0–10 kHz frequency range are available from 0046:49 UT to 0047:15 UT. An interference pattern started at the beginning of this data interval (0046:49 UT) and stopped about fifteen seconds later (0047:05 UT). The termination of the interference pattern corresponds exactly with the termination of the electron gun firing (DC mode). In the 0247–0250 UT FPEG event, the electron gun fired in the DC mode from 0247:29 UT to 0249:16 UT, followed by a break from 0249:16 UT to 0249:59 UT, and on again until 0250:45UT. The 0–10 kHz electric field data were measured during two times intervals. The first was from 0248:01 UT to 0248:27 UT, during which a clear interference pattern was visible over the entire time period. The second was from 0249:43–0250:09 UT, during which an interference pattern started in the middle (0249:59 UT) and stopped at the end (0250:09 UT).

During the 0411–0418 UT event, the electric gun was pulsed at 1.22 kHz with a 50–50 duty cycle. During this period, 0–10 kHz electric field wideband spectrums were measured 5 times, including the period from 0411 to 0412 UT shown in Figure 4.4. The influence of the antenna rotation can be seen, although the interference patterns are unclear and only partially formed. The interference patterns were only observed during one period (0411–0412 UT). During the period

from 0119 to 0120 UT, an unclear and partial interference pattern was observed in the 0–10 kHz range.

In order to confirm that the observed waves are electrostatic, a comparison was made between the electric field and magnetic field data. The wideband receiver was alternately connected to the electric antenna, the magnetic search coil, and less frequently to the Langmuir probe. Only a few frames of 0–10 kHz magnetic field data were obtained during periods when the electron gun was fired. No wideband 0–10 kHz magnetic data were obtained during the 0046–0047 UT event. The 0247-0250 UT event only included one period of 0–10 kHz magnetic data starting at 0250:35 UT. These magnetic field spectrograms show that a background of electromagnetic whistler mode radiation was present at a frequency of about 5 kHz from 0240 UT to 0258UT. This whistler mode radiation occurred both before and after the FPEG event and was clearly evident in both the electric and the magnetic wideband data. During the period when the electron gun was firing and 0–10 kHz electric field data were available, the 5-kHz whistler radiation was not visible in the electric field wideband spectrum, but remained visible in the magnetic field wideband data. Since the AGC permits only the strongest waves to be recorded, it is apparent that the beam associated electrostatic waves are much stronger than the background whistler mode radiation. No interference patterns were observed in the magnetic field data. Since the whistler mode waves are the dominant waves in the magnetic field data during the FPEG event, the beam associated waves must be electrostatic. During the 0411–0418 UT event, 0–10 kHz magnetic wideband data were obtained 5 times and only the AC modulation frequency (1.22kHz) of

the electron gun and its harmonics were observed. Therefore, in this event as well, the waves forming the observed interference patterns are electrostatic, and are similar to the waves observed in the 0046–0047 UT and 0247–0250 UT events.

During the 0330–0337 UT event, the electron gun was fired in the DC mode. No interference patterns were observed in the 0–10 kHz range, although strong electric field signals associated with the electron beam are present during this period. Since the electron gun was operated over a long interval, $\sim$ 7 minutes, many 0–10 kHz magnetic field spectra were obtained. By comparing the magnetic field wideband data with the electric field data, it is clear that the electric signals are caused by electromagnetic waves. During the 0047–0049 UT and 0120–0122 UT events, the electron gun was being operated in the ELF1 mode in which the electron gun was modulated at a variety of frequencies from $9.54 Hz$ to $610 Hz$. The electric and magnetic field wideband data during this period is dominated by signals that are generated by a beat between the electron gun pulsing and the repetition rate of the wideband spectrum analysis. Apparently these signals are due to electromagnetic whistler mode noise. No interference patterns were observed during this period. The electron gun also operated at many other times (0228–0236 UT and 0338–0400 UT) in either the ELF1 mode or the VLF1 mode. The electron gun was modulated at several different frequencies in the VLF range during these periods. No interference patterns and no intense electric field noise were observed during these time periods.

During the 0330–0337 UT and 0411–0418 UT events, the PDP passed near the magnetic conjunction point with the shuttle. The magnetic conjunctions occurred at 0333 UT and 0411 UT, respectively. During the 0046–0047 UT, 0119–0120 UT and 0248–0250 UT events, the PDP was not magnetically connected to the shuttle. The perpendicular distances between the PDP and the magnetic conjunction field line were 93 meters, 92 meters and 170 meters, respectively. During the 0330–0337 UT event when no interference patterns were observed, the PDP was on the upstream side of the shuttle. During the 0411–0418 UT event, when interference patterns were observed, the PDP was on the downstream side of the shuttle. Table 4.1 summarizes the characteristics of the electron gun operation with strong levels of low frequency (≤ 5 kHz) waves, and gives the characteristics of the observed interference patterns and the positions of the PDP relative to the shuttle. The coordinates X, Y and Z are the PDP position in the LVLH coordinate system centered at the shuttle. The distance R is the perpendicular distance from the PDP to the magnetic field line connected to the shuttle.

Interference Patterns Associated with Lower Hybrid Waves

During the 6-hour free flight mission, lower hybrid type interference patterns were observed more than 20 times in the 0–10 kHz and 10–20 kHz electric field wideband data. These interference patterns have different characteristics in the two frequency bands as shown in the Figure 4.5 for the 0038 UT event and in Figure 4.6 for the 0200 UT event. The U-shaped pattern always opens to lower frequencies in the 0–10 kHz band and to higher frequencies in the 10–20 kHz

band, and the interference patterns are always symmetric about the lower hybrid frequency (6–9 kHz). The lower hybrid frequency ω_{LHR} was computed using

$$\frac{1}{\omega_{LHR}^2} = \frac{1}{\Omega_{ce}\Omega_{ci}} + \frac{1}{\omega_{pi}^2} = \frac{m_{o+}}{m_e}\left(\frac{1}{\Omega_{ce}^2} + \frac{1}{\omega_{pe}^2}\right) \tag{12}$$

where Ω_{ce} is the electron cyclotron frequency, Ω_{ci} is the (oxygen) ion cyclotron frequency, ω_{pe} is the electron plasma frequency and ω_{pi} is the (oxygen) ion plasma frequency. In the Spacelab 2 environment, ω_{pe} is about three times Ω_{ce}. Therefore, the second term of right side of Equation (12) is a minor term. In this case, Equation (12) can be simplified as

$$\omega_{LHR} \approx \sqrt{\frac{m_e}{m_{O+}}}\Omega_{ce} \tag{13}$$

Therefore, the lower hybrid frequency can be obtained directly from the electron cyclotron frequency. Generally, the lower hybrid frequency is about 7–8 kHz. Therefore, the interference patterns in the 0–10 kHz band correspond to lower hybrid waves that are Doppler-shifted to lower frequencies (i.e., propagating upstream) while the 10–20 kHz interference patterns correspond to lower hybrid waves that are Doppler-shifted to higher frequencies (i.e., propagating downstream).

The wavevector direction in the X-Z plane can be determined from the center of the U-shaped pattern and the sense of the Doppler shift (up or down in frequency). In Figure 4.7 the wavevectors and magnetic field directions for the lower hybrid-wave interference patterns are plotted along the PDP's trajectory in the X-Z plane. The magnetic field direction is shown with a short line and the

wavevector direction is shown with a long arrow. Wavevector directions directed downstream and upstream correspond to interference patterns observed in the 10–20 kHz and 0–10 kHz bands, respectively. The plotted events all occur between 0124 UT and 0441 UT. Several similar interference patterns occurred either before or after this time period. However, since the PDP remained about 90 meters directly downstream from the shuttle and moved little relative to the shuttle during this period, these wavevector directions are not shown in Figure 4.7. The interference patterns all have characteristics similar to those shown in Figure 4.7. All these events are measured downstream from the magnetic field lines connected to the shuttle. This relationship suggests that the waves are produced by an interaction between the shuttle and the ambient ionosphere. The wavevectors derived from these events are nearly perpendicular to the magnetic field (in the X-Z plane). In most of the cases, the measured angles are within the ranges of $80 - 90°$, with $±5°$ error. Large wave normal angles relative to magnetic field, near $90°$, are an identifying characteristic of lower hybrid waves for plasma where $\omega_{pe} > \Omega_{ce}$. As we will show in the next section, the rest frame wave frequencies deduced from the interference patterns are very close to the lower hybrid frequency. From now on we refer to these interference patterns as lower hybrid-type interference patterns.

Comparing Figure 4.7 with Figure 2 of Gurnett et al. [1988], which demonstrated the strong noise region observed by the PDP's broadband receiver, we find that the lower hybrid-type interference patterns are strongly associated with high plasma wave intensities. Most of the interference patterns are observed in the

regions (dark dots in Gurnett et al.'s [1988] Figure 2) where the broadband shuttle-induced noise exceeds 1 mV/m. Measured power spectra at 0310UT and 0450 UT are shown in Figure 4.8. These spectra are obtained from the multi-channel spectrum analyzer which covers the frequency range from a few Hz to tens of MHz. The intensities around the lower hybrid resonance are clearly enhanced. The wave activity reaches the highest level around the lower hybrid resonance in the 0450 UT event and the second highest level during the 0310 UT event. The location of the lower hybrid-type interference patterns can be divided into two groups. The first group, which includes most events, were observed in the shuttle wake region when the PDP was about 100 meters downstream from the shuttle (from 0030–0130 UT and 0350–0455 UT), and when the PDP was approximately 250 meters downstream from the shuttle (from 0255–0312 UT). The second group, such as the 0200 UT and 0150 UT events, were observed when the PDP was approaching magnetic conjunction from the downstream direction. Both upward and downward Doppler shifts (corresponding to downstream and upstream propagation) were observed in each group of events.

An interesting new phenomenon observed in association with the lower hybrid waves is the occurrence of asymmetric or 'tilted' interference patterns. In these cases the U-shaped pattern is tilted either forward or backward in time (for example see the event at 0310 UT in Figure 4.9). This event is one of a series of lower hybrid-type interference patterns observed from 0250–0310 UT when the PDP was completing the last crossing well downstream from the shuttle. However, only the last one near 0310 UT was clearly asymmetric. This event occurred after

the PDP had crossed the wake region and the PDP's position along the z-axis had increased to about 140 meters in the shuttle rest frame. "Tilted" interference patterns were also observed at 0150 UT, 0200 UT, and 0325UT. These "tilted" interference patterns all occurred when the PDP had a relatively large Z position in the shuttle rest frame. Since the magnetic field is usually oriented somewhat out of the X-Z plane ($20 - 30°$), the PDP was not directly downstream from the shuttle at these times. The interpretation and simulation of these asymmetric interference patterns will be discussed in detail in the next section.

CHAPTER V

ANALYSIS OF THE ION ACOUSTIC-LIKE WAVES

Analysis

From the interference patterns in Figure 3.1 and Figure 4.3, the time when the nulls go to infinite frequency can be determined precisely. From Equation (5) it can be seen this condition occurs at $\phi = \pm\pi/2$ when the antenna is perpendicular to $\mathbf{k_{xz}}$, the projection of $\mathbf{k}$ onto the X-Z plane. From the antenna position at these times the angle between the projections of $\mathbf{V_{sc}}$ and $\mathbf{k}$ in the X-Z plane can be determined. This angle is either α or $\alpha + \pi$ with $\alpha \leq 90°$. The first solution, α, corresponds to a negative Doppler shift with the wave propagating in the upstream direction, and the second solution, $\alpha + \pi$, corresponds to a positive Doppler, with the wave propagating in the downstream direction. The Doppler term is the dominant term. By comparing the Doppler term, $k_{xz}V_{sc}\cos\alpha_k$, with the measured frequency, the sign of the Doppler term can be determined and therefore the direction of the wavevector $\mathbf{k}$ in the X-Z plane can be uniquely determined. The angle between the wavevector $\mathbf{k_{xz}}$ and $\mathbf{V_{sc}}$ is 150° for the 0046–0047 UT event and about 18° for the 0247–0250 UT event, respectively, with $\pm 2°$ error.

In the plasma rest frame the shuttle and the PDP move with speeds of 7.4 km/sec. These speeds are much larger than the speed of the PDP relative to

the shuttle (≤ 1 m/sec). The PDP's velocity relative to the shuttle can then be neglected when computing the Doppler shift. Since the angle between V_{sc} and k in the X-Z plane are deduced from the interference pattern, the Doppler shift term can be computed exactly. Subtracting the Doppler term from the measured frequencies at these null and maximum positions, the dispersion relation for $k_y = 0$ can be determined since $\omega_0 = \omega' + k \cdot V_{sc}$. For our cases the Doppler shift term is the dominant term, but since it is calculated precisely, the dispersion relation in the 2-D X-Z plane can still be deduced.

Using the method described above, constraints on the dispersion relation of the waves associated with the electron beam for the 0046–0047 UT and 0247–0250 UT cases have been determined. In order to determine the frequency of the null or maximum in the middle of the U-shaped pattern, we integrate over a fixed time interval centered on the center of the U-shaped interference pattern. For example, in Figure 3.1 a symmetry axis occurs near 0046:58 UT. A least squares fit is used to determine the frequency of each null and maximum as shown in Figure 5.1. Shown as a curve line in Figure 5.1, the function used in the fit is $\frac{\sin^2(x)}{x^2}$, which represents interference pattern effect in the electric field density spectrum as shown in Equation (10). The corresponding wavevector component k_{xz} for each null and maximum at the center of U-shaped can be determined from Equations (4) and (8). The Doppler shift and the rest frame frequency are then calculated exactly for each null and maximum, thereby leading to the dispersion relation in Figure 5.2. The errors are estimated as 0.1 kHz since the rest frame frequency is much smaller than the Doppler shifted term and the measured frequency in the

shuttle fest frame. As shown in Figure 5.2, the results for different integrating time intervals are very consistent. Noting that a very concentrated angular spectrum of waves is necessary for producing an interference pattern, we may argue that the fully three-dimensional dispersion relation should be very similar to Figure 5.2 with k_{xz} replaced by k. In this case the Doppler shift term $|\mathbf{k} \cdot (-\mathbf{V_{sc}})|$ is smaller than the observed frequency, implying that the wavevector $\mathbf{k_{xz}}$ has a component directed downstream from the shuttle. For the other event at 0247–0250 UT, we find the absolute value of the Doppler shift term $|\mathbf{k} \cdot (-\mathbf{V_{sc}})|$ is larger than the measured frequency ω'. This means that the waves are directed upstream for this event. The PDP is further away from the shuttle during this event ($\sim 210m$) than during the 0046–0047 UT event ($\sim 95m$). The wave intensities are so low that only one maximum and one null position can be clearly identified. The frequency in the plasma rest frame also increases with k_{xz} in the same frequency range as for the 0046–0047 UT event. In summary, the interference patterns for these events are both consistent with the waves having rest frame frequencies less than 600 Hz and a dispersion relation which is an approximately straight line. The last point in Figure 5.2 does not fit the linear relationship, possibly because of the rapid decrease in the electric field intensity in the high frequency range, as we show later in the power spectrum analysis. From the two-dimensional linear dispersion relation in Figure 5.2, the phase speed of the beam-associated waves can be estimated. Since the phase speed satisfies $V_s = \omega_0/k \leq \omega_0/k_{xz}$, the measured V_s deduced from the linear dispersion relation is less than 700 m/s.

The plasma in the vicinity of the space shuttle is primarily composed of ionospheric electrons and oxygen ions, and pick-up water ions formed by charge-exchange from water outgassing by the shuttle [Narcisi et al., 1983; Paterson and Frank, 1989]. Wherever confidence may be attached to the fitting routine, the data from the Retarding Potential Analyzer on the PDP spacecraft [Reasoner et al, 1988] imply an O^+ temperature of approximately 1000 K [Reasoner, private communication, 1989]. Electron temperatures of 2000-2500 K are often quoted for the Spacelab 2 mission [Murphy et al., 1989; Tribble et al., 1989]. Day-night variations and shuttle water effects imply that factor of two variations in the electron temperature can occur [Sisteind et al., 1984; Kohnlein, 1986; Murphy et al.,1989; Tribble et al., 1989; Pickett et al., 1989]. For the 0046-0047 UT FPEG event, the only one for which Langmuir probe data are available, $T_e \simeq$ 2500 K [Pickett, private communication, 1990]. This result could however be effected by the electron gun firing. Therefore, we take $T_e = 2000$ K. Water ion temperatures have not been measured. We therefore take $T_{H_2O+} \sim 300$ K, roughly the temperature of the shuttle, which is the source of the ions. The thermal speeds of the electrons, oxygen ions and water ions are then approximately $1.7 \times 10^5 \ ms^{-1}$, $720 \ ms^{-1}$ and $370 \ ms^{-1}$, respectively. The phase speed of ion acoustic waves in an unmagnetized plasma is

$$V_s = \sqrt{\frac{\kappa_B(T_e + 3T_i)}{m_{O+}}} \tag{14}$$

For the above electron/oxygen plasma, $V_s \simeq 1500 \ ms^{-1}$. Comparing the measured phase speed of the waves with these thermal speeds and the unmagnetized ion

acoustic speed, we can then conclude that the observed waves have phase speeds on the order of the oxygen ion thermal speed and one-half of the ion acoustic speed. Given the uncertainties involved, ion acoustic-like waves are a reasonable possibility. The angle between the measured wavevector $\mathbf{k_{xz}}$ and the magnetic field vector $\mathbf{B_{xz}}$ (projected onto the X-Z plane) is about 95° for both the 0046–0047 UT event and the 0248–0250 UT event. The true angle between $\mathbf{k}$ and $\mathbf{B}$ in three-dimensions should also remain large. These waves therefore propagate at a large angle relative to the magnetic field. Qualitatively the phase speed and the direction of propagation suggest that the waves are oblique ion acoustic-like waves.

The true power spectrum as a function of k_{xz} can be determined by eliminating the antenna interference effect using Equation (11). The result is shown in Figure 5.3 for the 0046–0047 UT event. A snapshot covering the period from 0046:57.6–0045:58.2 UT is used. The wave angular distribution is assumed to be a Gaussian distribution with a standard deviation of 4°. A standard deviation of 4° is chosen in order to get the best smooth fit over the entire power spectrum. The standard deviation is also consistent with the conclusion in the next section that the range of the wave propagation angles is less 10°. Accordingly, the rapid decrease in intensity for the measured spectrum is mostly due to the declining amplitude of the interference pattern with increasing frequency. For the true power spectrum, note that at the beginning the intensity increases with increasing frequency, reaching a maximum at around 4–5 kHz and then decreases rapidly. The deviation of the last point on the 2-D dispersion relation in Figure 5.2 below the

linear line is probably due to the decrease in the true power spectrum. Although the waves must propagate in a very concentrated range of angles, they evidently have a broad range of wave numbers.

Source Location and Wavevector Selection

When an electron beam is injected into a homogeneous plasma, a returning background electron flux is required to balance the electron beam current. This elementary notion has been confirmed in a series of plasma simulations performed by Okuda et al. [1987, 1988, 1990]. The returning electron flux has a net drift relative to the background ions, so that ion acoustic waves can be generated by the returning current. Ion acoustic waves can also be produced directly from the electron beam, for instance by the Buneman instability [Buneman, 1958] or as the decay products of beam-driven Langmuir waves. The close time correlation between continuous operation of the FPEG experiment and the observed ion acoustic-like waves implies that the ion acoustic-like waves are most likely generated either by the beam electrons directly or by electrons carrying a return current back to the shuttle. During both the 0046–0047 UT and 0247–0250 UT events, the waves propagate obliquely to the magnetic field and the component of the wavevector direction along the magnetic field line is most likely opposite to the direction of the electron beam motion as shown in Figure 5.4 and 5.5. This supports the hypothesis that the waves are being driven by return currents and not directly by the beam.

In the shuttle rest frame, the propagation velocity $\mathbf{V}$ of these waves is

$$\mathbf{V} = -\mathbf{V_{sc}} + \mathbf{V_g} \tag{15}$$

where $\mathbf{V_g}$ is the group velocity in the plasma rest frame. For ion acoustic-like waves with a straight line dispersion relation, the group velocity is equal to the phase velocity. Considering that the shuttle and the PDP are moving at 7.4 km/sec relative to the ionosphere, which is about 10 times the wave phase and group speeds, it follows that the ion acoustic-like waves must be primarily convected to the PDP by the streaming motion of the ionospheric plasma. If the waves are generated along the magnetic field lines intersecting the shuttle, they will take a time on the order of 10^{-2} second to reach the PDP, which is still much longer than the ion response time ($1/\omega_{pi}$), which is on the order of 10^{-4} second. If the ion acoustic speed is $700 ms^{-1}$, as indicated by Equation (14), then the waves would have time to travel only about 15 meters in the plasma rest frame. The PDP is about 93 meters away from field lines intersecting the shuttle during the 0046–0047 UT event and about 170 meters away during the 0247–0250 UT event. These estimates imply that the waves are generated within about ten meters of the magnetic field line through the shuttle.

Frank et al. [1989], using measurements of the electron velocity distribution on the PDP spacecraft, reported that a magnetically aligned sheet of electrons was observed in the wake of the shuttle at 0411:13–0412:02 UT, returning from a direction opposite to the propagation of the electron beam. During this time period the PDP was about 15 meters to 45 meters downstream from the magnetic field

lines intersecting the shuttle. The thickness of the sheet of returning electrons was about 20 meters. The hot returning electrons were also seen during the 0247–0250 UT event when the PDP was about 170 meters downstream of the magnetic field lines intersecting the shuttle. Apparently the returning electron sheet still exists a few hundred meters downstream from the shuttle. Presumably, ion acoustic-like waves associated with the return current could be generated throughout this volume. However, it is reasonable to believe that the most intense part of the returning hot electron flux travels along the magnetic field line intersecting the shuttle. It is also very likely that the ion acoustic-like waves are generated in this region and propagate at a very large angle with respect to the magnetic field line. The intersection point between V and B_{xz} is the most likely position for the ion acoustic-like waves to be generated in the X-Z plane. If the above argument is correct, during the 0046–0047 UT event the source of the observed waves is very close to the electron gun. The relevant geometry is shown in Figure 5.4. In this case the waves were propagating downstream. During the 0247–0250 UT event, the source was about 100 meters away from the shuttle. The relevant geometry is shown in Figure 5.5. In the shuttle rest frame the waves are traveling upstream, indicating the Doppler shift term is larger than the measured frequency. The rest frame frequency is therefore negative. In both of these cases, the observed wave vector directions and inferred source locations are consistent with the waves being driven by the return current electrons, and not directly by the beam electrons.

Although ion acoustic waves can be generated over a large range of positions along the magnetic field lines intersecting the shuttle, the waves observed by the

PDP spacecraft appear to be generated in a very localized area along the magnetic field lines. This is because the waves are primarily convected over the PDP by the ionospheric plasma flow ($V_g \ll V_{sc}$). Since the background plasma flow is along the negative x-axis, the wave generation region is near the intersection point between V_{sc} and B_{xx}. Using Equation (15), it can be shown that the observed waves must originate in a circle in the Y-Z plane, centered on the intersection point as shown in the Figure 5.6. Waves generated outside of the circle can not reach the PDP. Assuming the group speed is $700ms^{-1}$, the radius of the circle is about 10 meters for the 0046 UT event and about 18 meters for 0248 UT event, respectively. In both cases the magnetic field lines threading the shuttle intersect the circles as expected. Waves generated at different positions inside the circle must have different wavevector directions in order to reach the PDP and be observed. In other words, waves generated from each position can only have one unique propagation angle that can be observed by the PDP. On the other hand, the ion acoustic waves are likely to be generated in a significant source volume and not just one single point position. If a broad angular range of ion acoustic waves is generated, the PDP should have simultaneously observed waves with a broad distribution of wavevectors corresponding to different positions inside the circle. However, we show next that the observation of well-defined "fingerprint" patterns during the 0046–0047 UT and 0248–0250 UT events argue that the waves came from a very concentrated range of angles. This means that the waves, whether or not they are observed by the PDP, all have highly oblique wavevectors with respect to the magnetic field.

In order to determine how a concentrated distribution of wave angles could produce such well-defined interference pattern, a numerical simulation was performed to compare simulated interference patterns with the data. This simulation is shown in Figure 5.7. Here we assume that the wave angular distribution $F(\alpha_k)$ has a Gaussian distribution with a standard deviation varying from $1°$ to $10°$. These theoretical patterns are consistent with Equation (10), assuming that the real power density $E_0^2(k_{xz})/\Delta f$ is a constant. The spectra are computed by summing over hundreds of wave angles α_k. By comparing the numerical simulation with the observed interference patterns, we conclude that the range of wave propagation angles (two standard deviations), is less than $10°$.

If the waves are driven by the return current along the magnetic field lines intersecting the shuttle, oblique ion acoustic waves should be generated (and propagate) symmetrically at all directions around the magnetic field line. Projecting this cone of wavevectors on the X-Z plane, there should be two symmetric solutions, since the wavevector $\mathbf{k}_{xz}$ can point symmetrically on both sides of the magnetic field $\mathbf{B}_{xz}$ when $\mathbf{k}$ is almost perpendicular to $\mathbf{B}$. However, only one dominant angle is observed during both the 0046–0047 and 0248–0250 UT events. This asymmetry in the wavevector distribution is difficult to explain. Each wave propagation angle corresponds to a different source position. Although the other allowed source position on the same magnetic field line is within the wave-generating circle in the Y-Z plane for both events, it is further away from the shuttle than the observed source position. The best explanation of the asymmetric distribution of

wave normal directions is that the strongest waves are generated when the shuttle is closest to the magnetic field line through the source.

Linear Theory and Related Discussions

The FPEG events at 0119–0120 UT, 0330–0337 UT and 0411–0418 UT, have different characteristics than the 0046–0047 UT and 0248–0250 UT events. We do not observe a fingerprint pattern in the 0330–0337 UT event, although strong low frequency waves are visible in the Helios spectrum analyzer data. During this period the PDP approaches the magnetic conjunction from the downstream direction. Electromagnetic whistler mode radiation was observed during this event [Gurnett et al., 1986; Farrell et al., 1989]. The waves in the low frequency range are also most likely electromagnetic, since they were observed in both the electric and magnetic wideband data. No beam-generated electrostatic waves can be identified in the wideband data during this period. When the PDP was upstream from the shuttle (0334–0337 UT), the waves were carried away from the PDP by the background plasma (since $V_g \ll V_{sc}$). They did not have any possibility of reaching the PDP, since the PDP was upstream from the shuttle. When the PDP was downstream from the shuttle (0330–0333 UT), the PDP's Y position changed rapidly. The 0–10 kHz electric field spectrum was last measured at 0332:20–0332:46 UT just prior to the magnetic conjunction. At that time, the PDP was still more than 30 meters away from the magnetic field lines intersecting the shuttle in the Y-Z plane, which means it was out of the return current sheet region, so that the ion acoustic-like waves associated with the returning current

could not be observed during 0330–0333 UT. During the 0411–0418 UT event, the PDP was on the downstream side of the shuttle (after the magnetic conjunction with the shuttle). A poorly resolved interference pattern is observed in the 0–10 kHz frequency range in the wideband data during 0411:38–0412:04 UT. Although this pattern is not clear, it is similar to those observed during the 0046–0047 and 0248–0250 UT events. The wavevectors were also nearly perpendicular to the magnetic field. This means that the waves were also oblique ion acoustic-like waves, but with a much broader range of propagation angles than the first two cases at 0046–0047 and 0248–0250 UT. During this time period the PDP is close to the magnetic field line intersecting the shuttle and a current sheet of hot returning electrons was observed by Frank et al. [1989]. The PDP was therefore either inside or very close to the source region of the waves. In this case, the waves were detected by the PDP almost immediately after they were generated. It is therefore reasonable that waves with a broad range of propagation angles should be received during this period. The poorly resolved interference patterns may also be due to the fact that the PDP simultaneously received waves that were propagating both upstream and downstream. After the magnetic conjunction, the PDP rapidly moved backwards towards the original X-Z plane. The PDP was out of the wave generating circle in the Y-Z plane after 0412 UT, so that ion acoustic-like waves were observed only during the period 0411–0412 UT after magnetic conjunction. The explanation for the 0119–0120 UT case is more difficult, because the PDP is in the wake region, about 90 meters downstream from the shuttle. Apparently the ion acoustic-like waves generated along the magnetic field lines intersecting the

FPEG are observable by the PDP for a broad range of wave angles during this time period. The position of the PDP relative to the shuttle is close to but also slightly different than for the 0046–0047 UT event. Other low frequency electrostatic emissions were also observed before and during the electron gun firing. The expected interference patterns may have been obscured by these other electrostatic emissions.

ELF and VLF oscillations were also observed very close to the shuttle during Spacelab 1 electron beam firings [Neubert et al., 1986; Cai et al., 1987]. The ELF oscillations were found in the return current and the potential measurement, indicating that the spacecraft potential and the ambient return current oscillate at these frequencies. Neubert et al. [1986] found good evidence that these low frequency oscillations are most likely caused by a drift wave instability driven by density gradients in the plasma sheath around shuttle. However, the electrostatic waves discussed in this paper are most likely not drift waves. In the 0247–0250 UT event, the waves are generated in a small region (Figure 5.6) which is located more than 100 meters away from the shuttle along the magnetic field line. It is unlikely that the shuttle plasma sheath would persist to such distances. In addition, the drift wave instability results in an electric field power spectrum proportional to k^{-3} [Neubert et al., 1986]. This is not consistent with the shape of the power spectrum in the Figure 5.3.

Since the wavevectors are almost perpendicular to the magnetic field, $\sim 85°$, and the ion acoustic waves usually propagate at smaller angles to the magnetic field, the question arises: could these waves be ion cyclotron waves? (Cai et al.

[1987] have suggested that the low frequency fluctuations in the immediate vicinity of the shuttle are due to electrostatic ion-cyclotron waves.) The O^+ cyclotron frequency is about 30 Hz. Our measured wave frequencies in the plasma rest frame are up to 600 Hz, which is within the higher order O^+ cyclotron harmonics region. We cannot rule out the possibility that the waves are high-order ion cyclotron harmonic waves for two reasons. First, the frequency resolution of the instrument is comparable to the ion cyclotron frequency. Second and more importantly, since the Doppler shift is the dominant term, even a small spread in the wavevector directions could blur the harmonics together.

To investigate this issue we have used Vlasov linear theory to investigate the generation of low frequency electrostatic waves in a homogeneous, collisionless plasma with characteristics similar to those believed to be relevant for the electron beam events. The plasma is assumed to have three components: background O^+ ions with a Maxwellian distribution, beam electrons modelled either as a Maxwellian beam or a drifting ring distribution, and Maxwellian background electrons carrying a return current through a net drift along the magnetic field. The following plasma parameters were used: $n_e = n_{O^+} = 2 \times 10^4 cm^{-3}$, $n_b/n_e \sim 0.1 - 0.3$, $T_e = 2000$ K, $T_{O^+} = 1000$ K, $E_b = 1$ KeV, $V_b = 75 \; V_{te}$, and $\omega_{pi}/\Omega_{ci} = 200$. Here the subscripts e, O^+ and b refer to the background electrons, O^+ ions and FPEG beam electrons, respectively. The electrostatic dispersion equation is then of the form

$$1 + K_{O^+} + K_e + K_b = 0 \tag{16}$$

with

$$K_j = \frac{\omega_{pj}^2}{k^2 V_{tj}^2} \{1 + \sum_{-\infty}^{+\infty} exp(-\lambda_j) I_m(\lambda_j) Z(\zeta_j^m) \zeta_j^0\}.$$

Each dielectric constant K_i represents a magnetized Maxwellian distribution function for species j with unequal parallel and perpendicular temperatures. Here $I_m(\lambda_j)$ denotes the m'th order modified Bessel of the second kind with argument $\lambda_j = k_\perp^2 V_{tj}^2/\Omega_{cj}^2$, and $Z(\zeta_j^m)$ denotes the Fried-Conte function with argument $\zeta_j^m = (\omega - k_\parallel v_\parallel - m\Omega_{ci})/\sqrt{2}k_\parallel V_{tj}$.

The dispersion relation given by Equation (16) was solved for magnetized plasma conditions. When the drift speeds for the ambient electrons carrying the return current is small (0.3-0.7 V_{te}), lower order ion cyclotron harmonic becomes unstable while ion acoustic waves remain damped (Figure 5.8a). When the ambient electron drift speed increases to above 0.7 V_{te}, ion acoustic waves first become unstable parallel to the magnetic field. The ion acoustic mode becomes unstable at increasingly oblique wavevectors as the drift speed increases, reaching an angle characteristic of ion cyclotron waves $(85 - 88°)$ when the ambient electron drift speed reaches 0.8-1.0 v_{te} (Figure 5.8b,c,d). The growth rate of ion cyclotron waves is smaller than the growth rate of ion acoustic-like waves after the latter are generated. In addition, the maximum growth rate of the ion acoustic waves occurs for propagation parallel to the magnetic field. However, for the wavenumbers observed in the fingerprint patterns, the growth rates are slightly larger at highly oblique angles than at small angles relative to the magnetic field. By comparing the growth rate region with the measured power spectrum, it follows that the electron drift speed should be around V_{te}, where ion cyclotron waves are mixed

with the ion acoustic mode at the very large angles. This is also consistent with the measurements and simulations of Frank et al. [1989].

Figure 5.9 shows the dispersion relation and growth rate of waves with $\theta = 86.5°$ when $V_e = 1.0V_{te}$. The maximum growth regions of the ion cyclotron harmonic waves mimic the ion acoustic waves. The waves switch from the ion cyclotron mode to the ion acoustic mode as the wavenumber increases. At the same wavenumber, the wave switches from the ion cyclotron harmonic mode to the ion acoustic mode as the drift speed increases. As pointed out by Kindel and Kennel [1971], the highly oblique ion acoustic mode threads through the harmonic structure of the ion cyclotron modes. Therefore, for highly oblique propagation, ion cyclotron harmonic waves are similar and nearly indistinguishable from ion acoustic waves. The linear theory also shows that the properties of the beam electrons do not have much effect on the ion acoustic waves, which proves that the waves are produced by an interaction between the return current and the ambient O^+ ions. In summary, we find that ion acoustic-like waves should have large growth rates over a wide range of propagation direction. Thus, linear theory can provide highly oblique ion acoustic-like waves, but cannot explain the restricted range of wavevectors necessary to produce the observed interference patterns.

As discussed earlier, the measured phase speed for the waves is only about half the theoretical phase speed for unmagnetized ion acoustic waves. This discrepancy is addressed as follows. First, from the linear theory for magnetized electrons and oxygen ions we find that the phase speed of the unstable waves is lower than the unmagnetized ion acoustic speed for certain ambient electron drift

speeds. Secondly, both the 0046–0047 UT and 0248–0250 UT events took place in darkness (nightside), in which case the electron temperature may be lower than the assumed value of $2000K$, which would further decrease the estimated ion acoustic speed.

The generation of ion acoustic waves by an electron beam has been predicted by various studies. Okuda et al. [1988, 1989, 1990] and Pritchett [1990, and references therein] have simulated electron beam injection into homogeneous plasmas. They find that a return flux of background electrons is required to balance the beam current. This return electron flux drifts relative to the background ions, so that ion acoustic waves can be generated by the return current. Using one-dimensional numerical simulations, Okuda et al. [1988] showed that ion acoustic waves propagating parallel to the magnetic field can be excited when the ambient electrons carrying the return current have a much slower drift speed than the beam speed. Hwang and Okuda [1989] showed that oblique ion acoustic waves can be generated when the drift speed of the returning electron is very large relative to the ion thermal speed. More detailed two-dimensional and three-dimensional simulations have been performed by Okuda et al. [1988, 1990] and Pritchett [1990, and references therein]. These simulations are limited to the initial transient process associated with the electron beam injection, and do not discuss the ion response.

A second mechanism was proposed by Frank et al. [1989] based on the Spacelab 2 data. They suggest that the ambient electrons in front of the beam electron are forced to drift away from the shuttle due to a repulsive electric field at the front of the beam electrons. This drift of the background electrons relative

to the ions drives ion acoustic waves by the ion acoustic instability, and these ion acoustic waves provide a return flux of hot electrons by means of quasi-linear diffusion.

If the observed oblique ion acoustic-like waves are generated by a return current, then the component of the wavevector along the magnetic field should be in the same direction as the drift direction of the ambient electrons. Accordingly, the wavevector directions obtained from the fingerprint patterns allow us to determine whether the observed ion acoustic waves are driven by a return current of ambient electrons or by the ambient electrons drifting away from the front of the beam as suggested by Frank et al. [1989]. Figures 5.4 and 5.5 demonstrate that the wavevectors observed in the 0046–0047 and 0247–0250 UT events, respectively, are both consistent with a return current driving the observed waves by the ion acoustic instability and inconsistent with the mechanism proposed by Frank et al. [1989].

One problem that presently remains unresolved is the identification of the exact wave mode, i.e., whether the waves are ion acoustic waves or high–order ion cyclotron harmonic waves. The ion acoustic model experiences difficulties in explaining the severely restricted range of wave vectors directed at approximately 85° relative to the magnetic field. On the other hand, an interpretation involving ion cyclotron harmonic modes also encounters several problems. First, according to the linear theory, exciting the higher order ion cyclotron harmonic modes ($m \geq$ 10) requires a larger drift speed than for parallel ion acoustic waves. Once excited, the ion acoustic modes have larger growth rates than the ion cyclotron modes at

very large angle to the magnetic field. Second, if the waves are pure ion cyclotron harmonics, then the group speed for each harmonic mode is near zero, which means that the waves are observed by the PDP at approximately the place they are generated. Both upstream and downstream waves should be observed by the PDP. However, the observation shows the waves mostly propagate in one direction. In the 0046–0047 UT event, it is clear that only downstream propagating electrostatic waves are present in the wideband data. In the 0247–0250 UT event, although some evidence may suggest propagation in both directions, upstream waves dominate downstream waves. Considering the idealized nature of the linear theory and the debatable assumptions of spatial homogeneity and a Maxwellian distribution for the return electrons, the inability of the linear theory to explain all aspects of the observations is not unexpected. Indeed, since the ion acoustic and ion cyclotron harmonic modes tend to have very similar dispersion relations and merge together for oblique propagation, it is nearly impossible to distinguish between these two wave modes. They are often viewed as essentially the same mode.

CHAPTER VI

ANALYSIS OF THE LOWER HYBRID WAVES

Analysis

The lower hybrid waves observed during 0124–0441 UT have been shown in Figure 4.7 The angle between the wavevector and ambient ionospheric plasma flow direction (x-axis) has already been determined from the center of U-shaped interference patterns. For each maximum and null, the magnitude of the wavevector projected onto the X-Z plane k_{xz} can be determined from Equation (2) using the wave frequency measured in the shuttle rest frame. The motion of the PDP relative to the shuttle (~ 1 m/s) is much less than the shuttle speed (7.4 km/s) and can be neglected when calculating the Doppler shift. By subtracting the Doppler shift term, $k_{xz}V_{sc}\cos\alpha$, the wave frequency in the ambient ionospheric plasma frame can be deduced from Equation (3) for each maximum and null. These wavenumbers and frequencies allow a determination of the dispersion relation of the wave in the ambient plasma rest frame. The dispersion relation for the waves near 0038 UT is shown in Figure 6.1. The rest frame wave frequencies are very close to and a little above the lower hybrid frequency ω_{LHR}. The errors are estimated as 0.1–0.2 kHz. The thin line in Figure 6.1 is the cold plasma dispersion relation of lower hybrid waves (see Appendix). As can be seen, the lower hybrid waves observed by the PDP are in the flat dispersion relation range. The

deduced dispersion relation is consistent with the cold plasma theory. Dispersion relations have also been deduced for the 0128 and 0200 UT events where interference patterns are clearly presented. Both upstream (0200 UT) and downstream (0038 and 0128 UT) propagating waves have similar characteristics to these shown in Figure 6.1. The other interference patterns are not clear enough to compute the dispersion relation. Usually only one or two nulls or maximums can be determined. Nevertheless, the rest frame frequency can still be computed from these nulls or maximums. From the approximately ten interference patterns that were measured it is found that the wave frequency is always very close to the lower hybrid frequency in the plasma rest frame.

Using the same technique as for the ion acoustic-like waves (Chapter V), the relative power as a function of wavenumber (or wavelength) can also be determined for each interference pattern. This spectrum only covers the wideband frequency region (0.4–20 kHz) and includes only relative intensities because the AGC eliminates absolute intensity information. The true power spectrum $E_0^2(k_{xz})$ was computed from the measured power spectrum using Equation (4) to eliminate interference effects. The degree of clarity of the interference pattern depends on the angular distribution of wavevectors $F(\alpha_k)$ (for the same wavenumber). A Gaussian distribution is assumed for the wave angular distribution $F(\alpha_k)$ when we deduce the true power spectrum. The variable standard deviation is minimized in order to find the best fit to the angular distribution. Therefore, both the power spectrum and the angular distribution of the waves $F(\alpha_k)$ can be determined from the best fit. Figure 6.2 shows the best fit power spectrum for the 0038 UT event.

The waves have a standard deviation in the angle α_k of 5°. The range of wavelengths for the lower hybrid waves is about 1–4 meters, with the intensity peaking near 2 meters.

"Tilted" Interference Patterns

Most of the interference patterns have a vertical symmetry axis through the center of the U shape. This occurs whenever waves with different wavelengths have the same wavevector direction. However, as shown in Figure 4.9, in some cases asymmetric or "tilted" interference patterns were observed by the PDP. Such "tilted" interference patterns have never been reported before. Asymmetric interference patterns can occur when waves with different wavelengths have angular distributions centered at different propagation directions in the X-Z plane. In this case the angle α_{k0} becomes a function of wavenumber k_{xz}. Different nulls and maxima are then centered at different times or angles ϕ, which makes the U-shaped pattern tilt. Therefore "tilted" interference patterns can be formed. A theoretical simulation of a "tilted" interference pattern is shown in Figure 6.3. This pattern is based on Equation (11) with a constant electric field $E_0(k_{xz})$ and the angle α_{k0} varying linearly with the wavenumber k_{xz}. The rest frame frequencies are assumed to be constant at the lower hybrid frequency (8 kHz) with a downward Doppler shift in the shuttle rest frame. A Gaussian distribution with 5° standard deviation in α_k is assumed for $F(\alpha_k)$ in Equation (11). The overall change in angle α_{k0} is less than 15° for the range of observable wavenumbers in Figure 6.3. As can be

seen, even for this simple linear model, the calculated shape agrees very well with the observed shape.

Variations in the wave vector and group velocity direction as the function of wave number are the fundamental reason that "tilted" interference patterns can occur. Geometry and propagation effects almost certainly play a role in forming "tilted" interference patterns. For the lower hybrid waves, the wavevector direction is almost perpendicular to the magnetic field. The angular variation for different wavenumbers is very small, usually less then $1-2°$. If the waves propagate close to the X-Z plane and are perpendicular to the magnetic field, the wavevector projected onto the X-Z plane would point in the same direction for all wavenumbers. Therefore, one can argue that waves propagating primarily in the X-Z plane cannot form a "tilted" interference patterns. The component of the wavevector k_y has to be quite large for "tilted" interference patterns. For lower hybrid waves, the group velocity varies with the wavenumber. Waves with different wavelengths are therefore likely to come from different source regions. When the wavevectors are projected onto the X-Z plane, waves from different source regions propagate in different directions. The direction may vary a significant amount if k_y is large enough. This general explanation is consistent with the observations since all the "tilted" interference patterns are observed when the PDP had a relatively large Z position in the shuttle rest frame (i.e., when the PDP was not directly downstream from the magnetic field lines threading the shuttle). During these events the PDP is therefore not directly downstream from the ion cloud outgassing from the shuttle, which is the likely source region of the lower hybrid waves [Cairns

and Gurnett, 1991a,b]. For the 0310 UT event (Figure 4.9), the magnetic field direction is about 30° out of the X-Z plane. In the Y-Z plane the PDP was 50–60 meters along the y-axis from the point which at magnetic conjunction with the shuttle. This geometry suggests that the waves propagated about 70–80 meters in the ambient plasma rest frame and convected about 150 meters along the x-axis, assuming that the waves were generated near the magnetic conjunction with the shuttle. For this geometry the group speed of the waves would be about half the shuttle speed relative to the ambient ionospheric plasma V_{sc}, which is about ten times the ion thermal speed. Such high group speeds are unlikely for the lower hybrid waves which has a flat dispersion relation as shown in Figure 6.1. Therefore in this case, the source region is not in near field zone, but some local region along the x-axis through the PDP.

Lower Hybrid Waves Associated with Thruster Firings

The shuttle's thrusters were fired frequently during the PDP free flight period. The thruster firings cause the yellow spikes at extremely low frequencies in the color-coded broadband spectrum shown in Figure 6.4. These spikes can also be seen in the wideband data, for instance at 0200:19 UT in Figure 4.6. The density of neutral gas produced from the thruster firing can reach $10^8 cm^{-3}$ locally, which is a thousand times higher than the ambient plasma density. The correlation between the amplitude of the electrostatic waves and thruster firings has been studied by Gurnett et al. [1986]. Although most of the lower hybrid waves are not directly related to thruster firings, many of lower hybrid-type interference patterns

are observed during times of high thruster activity. We also found some cases in which thruster firings were directly responsible for the observed lower hybrid waves, for example near 0323 and 0326 UT in Figure 6.4. During these times the PDP was approaching a magnetic conjunction with the shuttle. The background electric field levels were relatively low. Right after the thruster firings, which lasted for less than a second, the lower hybrid waves were clearly enhanced for about 20 to 30 seconds. Since the neutral gas released from thruster firings has a much higher density then the ambient ionospheric plasma, it is clear that thruster firings should enrich the shuttle water cloud for a considerable period of time, thereby enhancing the level of lower hybrid waves driven by pick-up ions for some times. Both water vapor outgassed from the shuttle and neutral gas produced by the thruster firings apparently contribute to the neutral water cloud surrounding the shuttle. The relative contributions of the thruster firings and outgassing from the shuttle is poorly understand and needs to be investigated further.

Comparison with Previous Theoretical Work

The lower hybrid waves are likely generated by the ambient ionospheric plasma interacting with the neutral gas surrounding the shuttle [Gurnett et al 1988, Paterson and Frank 1989, Cairns and Gurnett 1991a,b]. As described above there are two major sources contributing to the neutral water gas cloud. One is the steady outgassing of water molecules from the shuttle, and the other is shuttle thrusters. Cairns and Gurnett [1991a] pointed out that the amplitude and spectral character of the low frequency electrostatic waves observed during

the PDP free flight was controlled by the angle between the magnetic field and the shuttle velocity relative to the ionospheric plasma. When the shuttle velocity is approximately perpendicular to the magnetic field, large wave amplitudes and the characteristic "mushroom" shaped frequency-time structures are observed in the broadband spectrum (see the semi-log scale plot in Figure 6.5), whereas more nearly parallel flows are characterized by low wave levels. The top line of the "mushroom" is near the lower hybrid frequency. The base of the "mushroom" is a triangular-shaped emission which starts at low frequencies and extends up to the lower hybrid frequency near the center of the "mushroom". For the observed broadband spectrum, see Plates 1 and 2 of Cairns and Gurnett [1991a]. The correlation between the spectral features of the mushroom and the magnetic field angle has a natural interpretation in terms of the optimum conditions for wave growth driven by pick-up ions and the time available for evolution of the wave spectrum [Cairns and Gurnett 1991a]. The pick-up ions are produced from the outgassing water molecules though collisional charge exchange processes with ionospheric O^+ ions [Paterson and Frank, 1989; Cairns 1990]. When the shuttle velocity has a significant component along the magnetic field, the pick-up ions will quickly separate from the ambient ionospheric plasma flow and convected waves. The pick-up ions will then have little time to interact with the the ambient ionospheric plasma and the waves.

Cairns and Gurnett [1991b] studied the characteristics of the near zone waves observed within 10 meters of the shuttle during the Spacelab 2 mission. At

that time the PDP was attached to the RMS arm and remained in the same position (about 10 meters away) relative to the shuttle. As shown by the dashed curve in Figure 6.6, the relative electric field spectrum of the near zone waves (average over 25 minute interval 0145–0210 UT, Day 212, 1985) has three components: one peak near the lower hybrid frequency, another peak at lower frequencies (about 200 Hz) and a solid uniform component between the two peaks. On the other hand, the solid line in Figure 6.6 is the relative electric field spectrum measured over 1 minute interval (0304:45–0305:45 UT, Day 213, 1985) at the center of the "mushroom" during the free flight mission. The average absolute spectral density for both cases is shown in Figure 6.7. As can be seen, the waves observed in the near zone and the waves observed during the free flight have quite similar density spectra and are within the same intensity range. In the free flight case, the relative electric field spectrum also has a peak around the lower hybrid frequency and a similar uniform region, but the peak at the lower frequencies is diminished. These similarities strongly imply that the waves observed at the center of the "mushroom" are also generated in the near zone region. The difference at the low frequencies peak between the two cases implies that the lower frequency waves may be heavily damped. Thruster firings may also enhance the lower frequency peak in the near zone case. Note that no thruster firings occur during the free flight period chosen.

Cairns [1990] has established a model for the water ion distribution surrounding the shuttle based on the observations by Paterson and Frank [1989]. A distribution of water ions in the form of a beam arc distribution is formed in the

vicinity of the shuttle. This distribution, which has both ring-like and beam-like characteristics, varies with distance from the shuttle: it is a ring far from the shuttle and is strongly beam-like distribution very close to the shuttle. Cairns and Gurnett [1991a,b] proposed that the waves observed in the "mushroom" structures and the near zone region are Doppler-shifted lower hybrid waves driven by ring and beam distributions of pick-up water ions, respectively. In the shuttle rest frame, the beam-driven waves are Doppler shifted downward to a lower frequency range. Linear theory shows that the beam-driven waves cover the entire frequency range from zero frequency to ω_{LHR}. The wavelengths are 1-4 meters and within the detectable range of the plasma wave antenna on the PDP. The waves also propagate almost perpendicular to the magnetic field, as expected. Linear theory also shows that the beam distribution has a broader growth region and tends to apply to the uniform region between the two peaks. On the other hand, the ring distribution tends to produce waves primarily at lower frequencies, perhaps explaining the low frequency peak around 200 Hz. These linear analyses assumed that the shuttle velocity is exactly perpendicular to the magnetic field. Cairns and Gurnett [1991b] suggested that nonlinear and other effects may produce the peak localized near the lower hybrid frequency ω_{LHR}. Cairns and Gurnett [1991a] also suggested that the waves are produced both very near to the shuttle and throughout the region with pick-up ions.

Based on the theory of Cairns and Gurnett [1991a,b], Rivas and Hastings [1992] have done further work on the near zone waves for a beam arc distribution. Their theory is linear, and a series of beamlets were used to make up a

homogeneous beam-arc distribution. The beam-arc is finite and has a distribution angle $\Delta\Theta$. For small arcs, $\Delta\Theta < \Delta\Theta_{crit} \approx 60°$, Rivas and Hastings [1992] consider the beam-arc plasma instability to be hydrodynamic, while for arcs larger than $\Delta\Theta_{crit}$ it is kinetic. Their linear analysis also assumed the shuttle velocity to be exactly perpendicular to the magnetic field which is rarely true during the Spacelab 2 mission. Usually the magnetic field direction is $20 - 30°$ out of the X-Z plane. In order to distinguish the difference between the theory and the true situation, we replace the theoretical X-Z plane of Rivas and Hastings [1992] with the X'-Z' plane. the x'-axis is same as the x-axis in the LVLH coordinate system, but the z'-axis is along the magnetic field direction. The waves which propagated out of the X'-Z' plane were also investigated. The critical angle $\Delta\Theta_{crit}$ is larger for waves propagating out of the X'-Z' plane. For finite beam-arcs this dependence causes waves propagating within the X'-Z' plane to be kinetic while waves propagating out of the X'-Z' plane are more likely to be hydrodynamic. They grow in different wavenumber regions and are Doppler-shifted into different frequency regions. Therefore, they interpreted the top cap of the "mushroom" as lower hybrid waves propagating within the X'-Z' plane while the base of the "mushroom" is interpreted in terms of lower hybrid waves propagating out off the X'-Z' plane.

The lower hybrid type interference patterns observed in the wideband data correspond to the "uniform" and "lower hybrid" components defined by Cairns and Gurnett [1991 b]. Since the 0–10 kHz wideband channel has a lower cutoff at 400 Hz, no information is available on Cairns and Gurnett's low frequency component near 200 Hz. As mentioned in the last section, lower hybrid type interference

patterns can be divided into two groups. The first group consists of interference patterns observed directly downstream the shuttle while the second group consists of interference patterns observed near the magnetic conjunction with the shuttle. Most of the observed lower hybrid type interference patterns belong to the first group. The second group includes the few "tilted" interference patterns observed. Since the group speeds of the lower hybrid waves are small compared with the shuttle speed, the waves are mostly convected downstream to the PDP by the ambient ionospheric plasma. The first group is observed almost directly downstream from the shuttle. The source region of these waves should be located in the near vicinity of the space shuttle where the neutral gas density is constantly large. Our observations indicate that the source region is likely to be within 20 meters of the shuttle. This implies that convection of the waves generated in the near vicinity of the shuttle is the dominant source of waves observed downstream from the shuttle as suggested by Cairns and Gurnett [1991a,b]. Note that the waves observed near the magnetic conjunctions also correspond primarily to near zone waves with $k \perp B$ since the E fields of these waves vary slowly with distance along the magnetic field line [Cairns and Gurnett, 1991b].

As mentioned before, the second group, consisting of "tilted" interference patterns, is not likely to be generated near the magnetic field conjunction with the shuttle and is most likely composed of the waves that are propagating significantly out of the X-Z plane. On the other hand, the interference patterns in the first group correspond to near zone waves that mostly propagate within the X-Z plane (since they are symmetric interference patterns). The observation of interference

patterns in the first group supports Rivas and Hastings's interpretation [1992], in which the cap of the "mushroom" figure is caused by lower hybrid waves generated in the near zone and propagated mostly within the X'-Z' plane. However, the interference patterns can not provide any information on Cairns and Gurnett's [1991b] lower frequency peak since the lower cutoff of the 0–10 kHz channel is 400 Hz. No interference patterns can be identified in the 40–1000 Hz channel, but this channel may be too narrow for interference patterns to be clearly identified. We do have evidence that lower hybrid waves propagate out of X-Z plane in the form of "tilted" interference patterns. However, they are not generated in the near zone region of the shuttle. Waves of this type are not considered in Rivas and Hastings's [1992] theory. Therefore, we can not say whether the lower frequency peak corresponds to the lower hybrid waves propagating out of X'-Z' plane as proposed by Rivas and Hastings [1991].

Another significant difference between the linear theory and the data is the dispersion relation of the waves. The frequencies of the observed lower hybrid waves lies very close to and a little above the lower hybrid frequency (ω_{LHR}) in the plasma rest frame and is essentially independent of wavenumber. However, the linear theory [Cairns and Gurnett, 1991a,b] shows that the waves can be generated over the entire frequency range from 0 to ω_{LHR} (also in the plasma rest frame) with a beam-like dispersion relation ($\omega_r \sim kV_{sc}$). This difference can be addressed qualitatively in terms of the evolution of the lower hybrid instability: as the instability saturates, the waves may evolve from the dispersion relation given by the linear theory to the dispersion relation of the lower hybrid mode (in the ambient

plasma). This idea is supported by (1) results of Nishikawa and Cairns [1991] for electron beam-driven Langmuir waves, and (2) the strong analogy between the ion beam-driven lower hybrid instability and the electron beam instability for Langmuir waves [Papadopoulos, 1984; Cairns and Gurnett, 1991b].

CHAPTER VII

CONCLUSIONS

Antenna interference pattern effects were frequently observed in the PDP plasma wave data during the Spacelab 2 flight. Analysis of the antenna interference patterns generated by these waves permits a determination of the wavelength, the direction of propagation and the location of the source region. Two types of interference patterns were observed: one corresponding to waves with very low frequencies (a few hundred Hz) in the plasma rest frame and the other corresponding to waves near the lower hybrid frequency.

The first type of interference pattern is clearly associated with electron beam firings from the shuttle. Strong low frequency (below 10 kHz) electron field noise was observed in the wideband data during two periods in which an electron beam was being ejected from the shuttle. This noise shows clear evidence of interference patterns caused by the finite (3.89 m) antenna length. The low frequency noise was the most dominant type of noise produced by the ejected electron beam. The observed waves have a linear dispersion relation very similar to that of ion acoustic waves. The wavelengths are relatively short, about 1–4 meters. The group and phase speeds of the waves are about 700 m/s. The source region has also been determined. The waves are believed to be oblique ion acoustic or high-order ion cyclotron waves generated by a current of ambient

electrons returning to the shuttle in response to the ejected electron beam. This work therefore provides direct observational evidence that ion acoustic waves can be driven by injecting electron beams into a plasma, as has long been be predicted on the basis of theory and simulations.

The second type of interference pattern is associated with lower hybrid waves driven by pick-up ions from the water vapor cloud around the shuttle. These waves are generated mostly in the near vicinity of the shuttle. "Tilted" interference patterns also suggest that some of these waves are generated well away from the shuttle. The wavelengths are also relatively short, about 1–2 meters. The frequencies in the plasma rest frame are very close to the lower hybrid frequency and the waves have an essentially flat dispersion relation. The interference pattern analysis implies that the waves are Doppler-shifted lower hybrid waves, thereby confirming Cairns and Gurnett's [1991a,b] identification of the wave mode and the qualitative details of the instability. The interference patterns correspond to the peak around the lower hybrid frequency and the uniform component between the two peaks identified in the broadband spectrum by Cairns and Gurnett [1991b]. The differences between the linear theory and the observational data suggest that the waves evolve into a frequency spectrum with $\omega \sim \omega_{LHR}$. So far all the theoretical investigations have been limited to cases in which the magnetic field is exactly perpendicular to the space shuttle velocity, which is rarely true during the PDP free flight mission. This may severely limit the applicability of the present linear theories since the magnetic field component along the shuttle velocity direction may play an important role in both the generation and propagation of the

lower hybrid waves. Further work is needed to understand the details of the wave spectrum and the time evolution of the lower hybrid instability.

Table 2.1: Plasma Parameters During the PDP Free Flight

parameter	value	unit
B	0.2–05	Gauss
n_e	2×10^4	cm^{-3}
T_e	2000	K
$T_{H_2O^+}$	300	K
T_{O^+}	1000	K
$\mathbf{V}_{sc}$	7.4	km/s
V_{te}	0.2	eV
R_i	3	meters
ω_{ce}	0.8–1.2	MHz
Ω_{ci}	25–35	Hz
ω_{pe}	2–3	MHz
ω_{LHR}	6–9	kHz

Table 4.1: FPEG Experiments During the PDP Free Flight

Beam Time (UT)	Beam Type	Fingerprint	X(m)	Y(m)	Z(m)	R(m)
0046:11-0047:05	DC	CLEAR	-95	-4	-5	93
0047:31-0049:16	ELF1	NONE	-96	-4	-4	89
0119:23-0120:17	DC	UNCLEAR	-92	-2	-1	92
0120:33-0123:18	ELF1	NONE	-96	0	-7	98
0247:29-0249:16	DC	CLEAR	-209	-25	-108	161
0249:59-0250:53	DC	CLEAR	-215	-22	-95	172
0330:12-0337:22	DC	NONE	55	-92	189	15-30
0411:13-0417:24	1.22kHz	UNCLEAR	-144	-53	-156	2-30

Figure 2.1: Identification of the various instruments carried

by the PDP.

D-G8I-377-I

400 MHz TELEMETRY ANTENNAS

ELECTROMETER

PRESSURE GAUGE

HF ANTENNA

ION MASS SPECTROMETER

LEPEDEA

DIFP
RPA

SEARCHCOIL

IMS

HF ANTENNA

AC-DC ELECTRIC ANTENNA

AC-DC ELECTRIC ANTENNA

LEPEDEA

RPA/DIFP

LANGMUIR PROBE
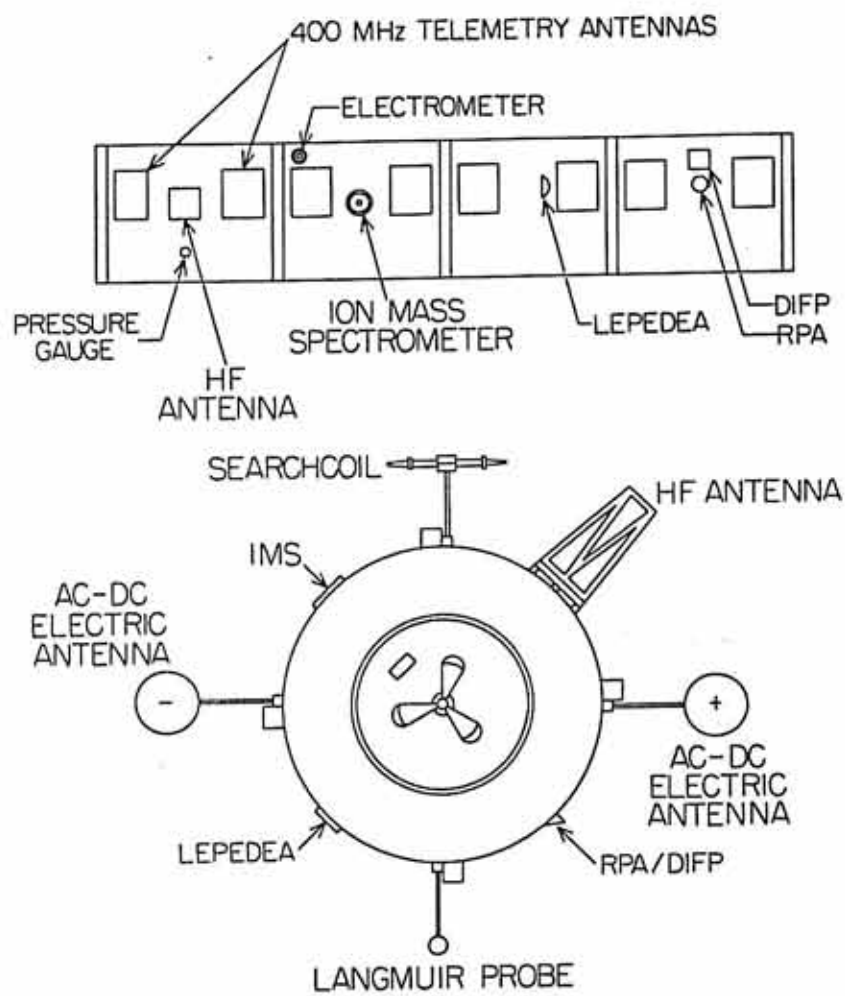
Figure 2.2: One complete antenna sequence for both the PDP ELF and VLF wideband data.
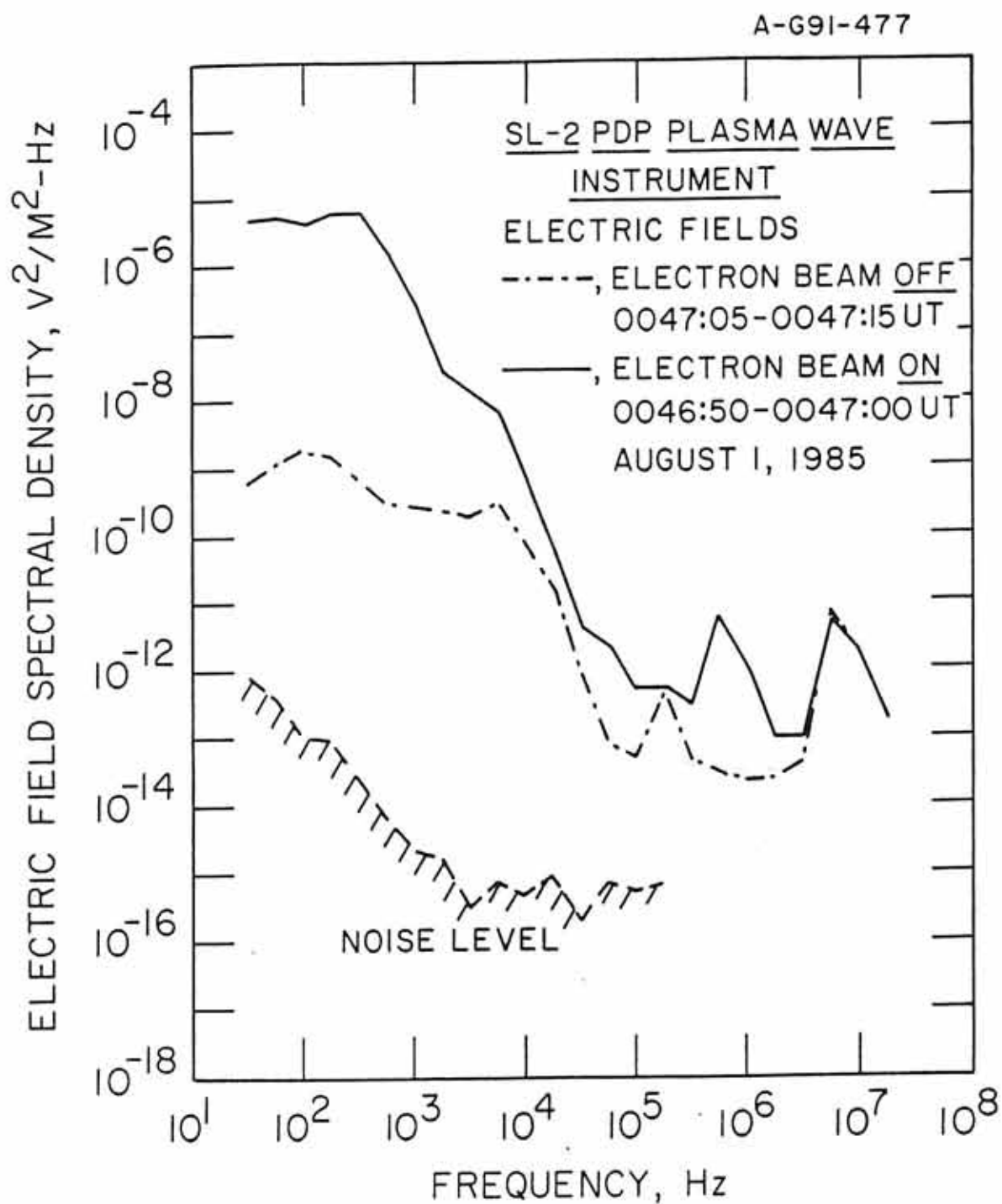
PDP WIDEBAND DATA

ONE COMPLETE ANTENNA SEQUENCE

A-G90-519

Figure 3.1: An example of an interference pattern observed in the
0–10 kHz electric field wideband spectrum. This frequency-time
spectrum was obtained over a 13-second interval (0046:50–0047:03 UT)
on August 1, 1985. The PDP spacecraft spin period at this time was
13.6 seconds.

A-G90-432

FREQUENCY, Hz

PDP, AUG. 1, 1985
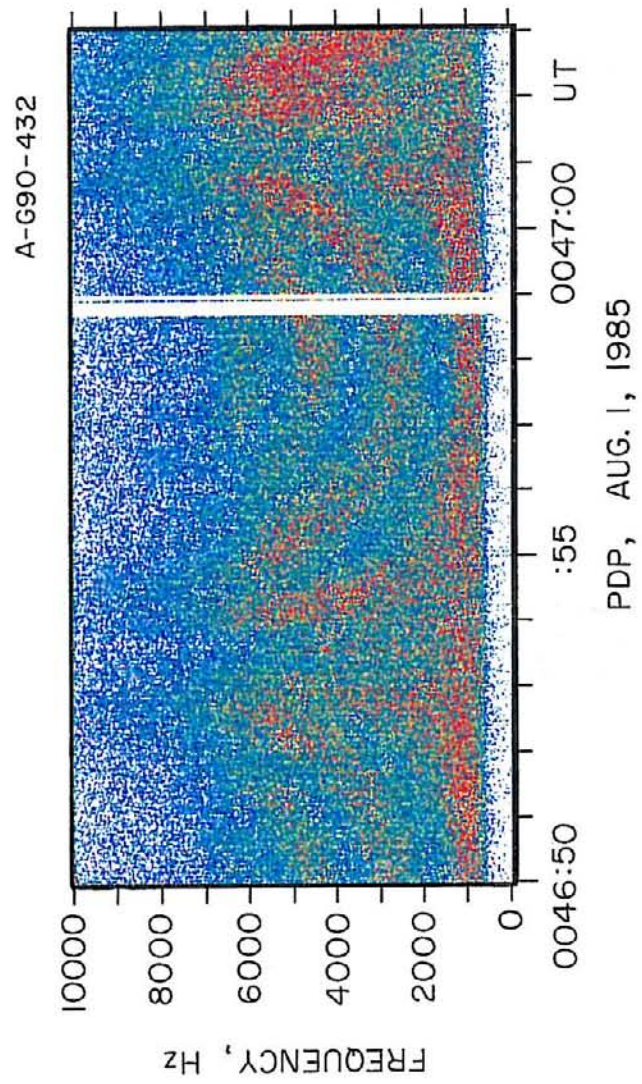
Figure 3.2: The position of the PDP antenna in the LVLH coordinate system. The z-axis in the LVLH system lies along the geocentric radius vector to the spacecraft and is positive toward the center of the Earth. The x-axis lies in the orbital plane and is positive in the direction of spacecraft motion. The y-axis is normal to the orbital plane and completes the right-handed orthogonal system. The electric antenna is rotating in the X-Z plane.

69

A-G90-442

LVLH COORINATES
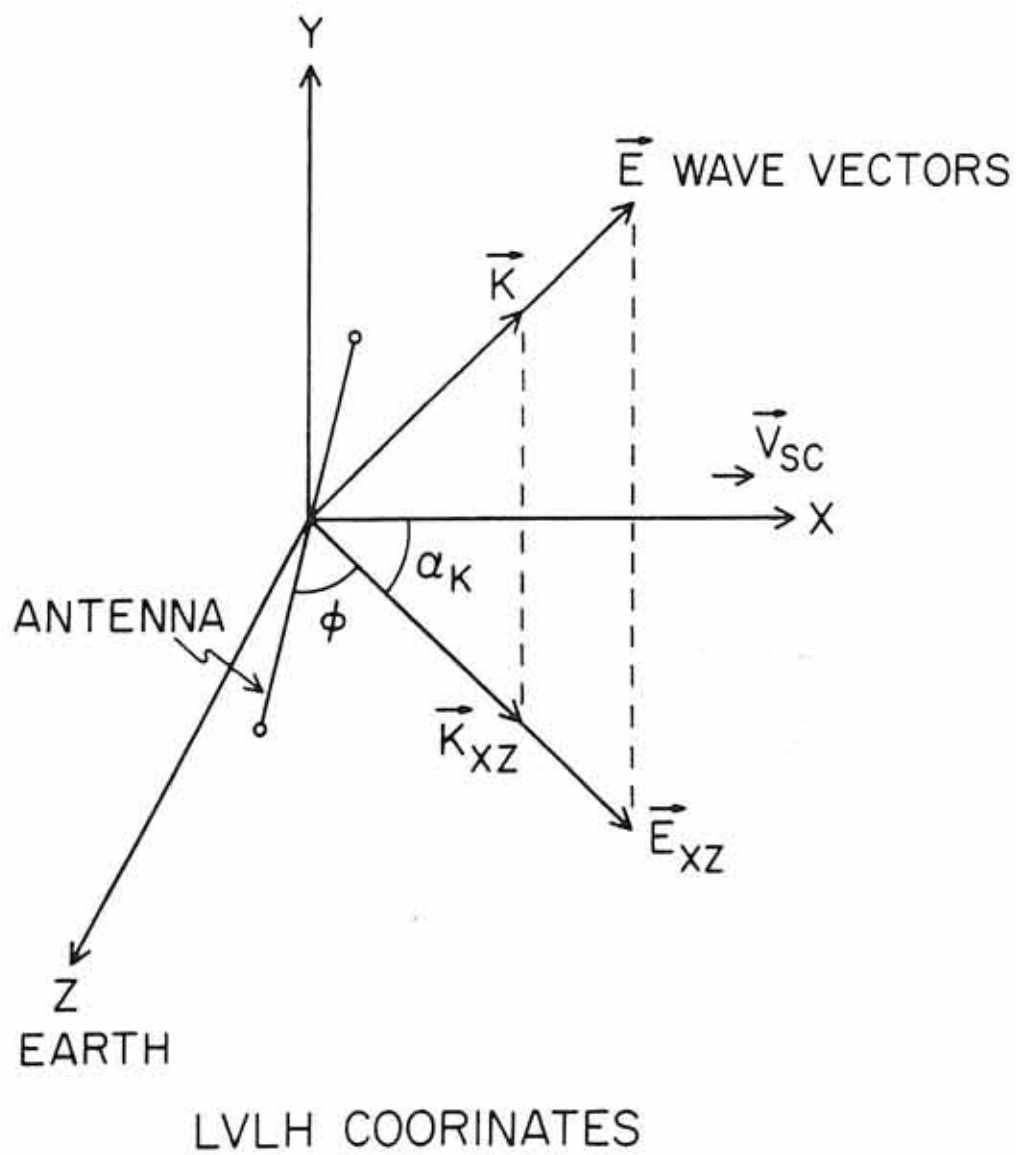
Figure 4.1: A broadband electric field spectrogram from the Helios
and MFR data for the time periods 0046–0047 UT, 0119–0213 UT,
0247–0251 UT and 0411–0419 UT. The electric field spectral
density, $E^2/\Delta f$ where Δf is the bandwidth of the filter
channel, is color-coded with blue being the least intense and red
being the most intense. The white curves labelled f_{ce} and f_{LH}
are the electron cyclotron and the lower hybrid frequencies,
respectively. The intense (red and yellow color) waves below
about 5 kHz are the waves associated with the injected FPEG electron
beams. In each of the four events shown in this figure, complete or
partial antenna interference patterns are found in the 0–10 kHz
electric field wideband data.

B-G90-433

LOG_{10} ($E^2/\Delta f$), $VOLTS^2$ m^{-2} Hz^{-1}
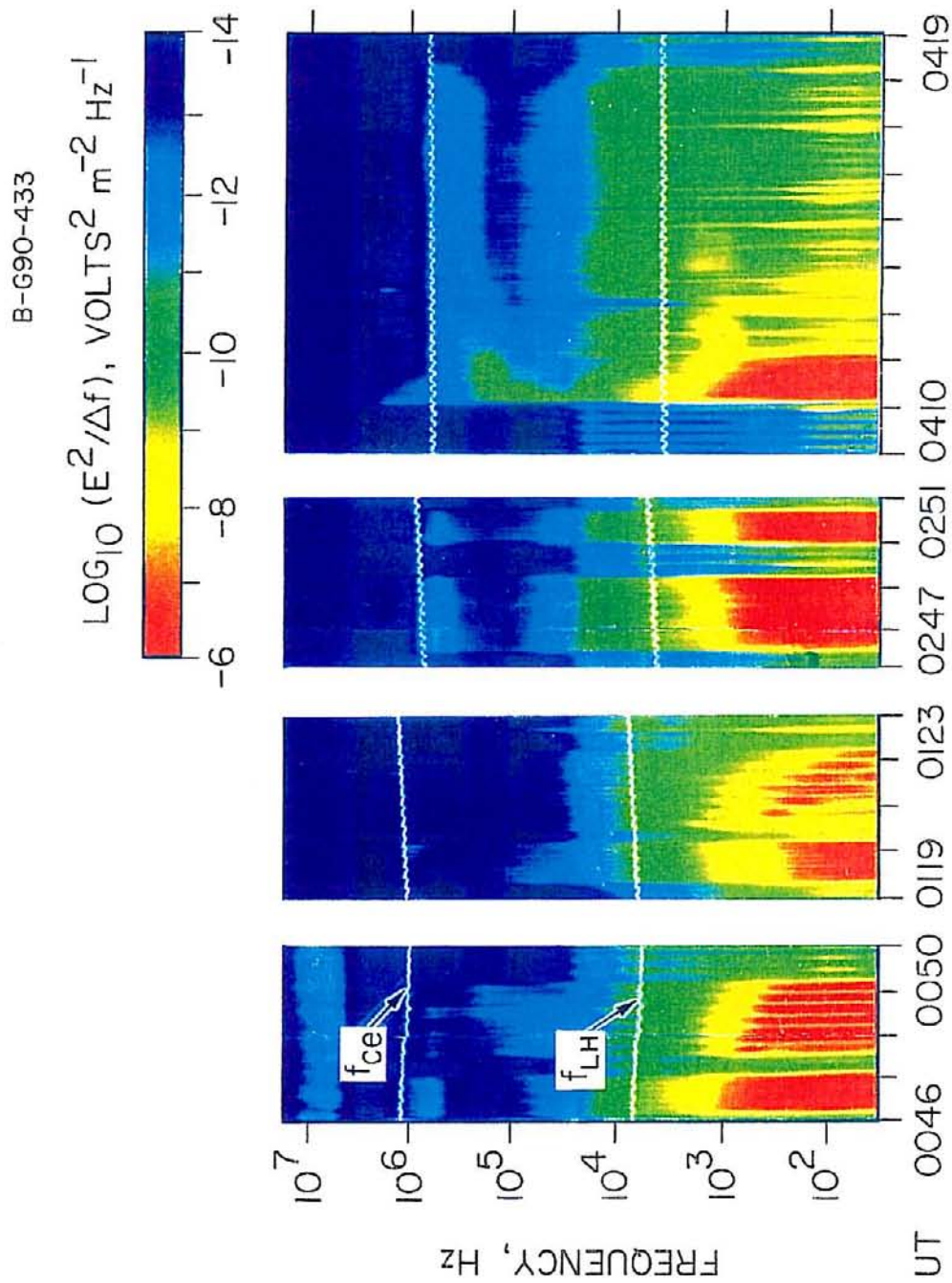
PDP, AUG. 1, 1985

Figure 4.2: The electric field spectral density as a function of the frequency during the 0046–0047 UT event and the comparison with the electron beam off and the background noise level. As shown when the electron beam is on, the spectral density increases significantly in the very low frequency region and near the electron plasma frequency region.

A-G9I-477

Figure 4.3: Another example of an interference pattern observed in the 0–10 kHz electric field wideband spectrum. This is a frequency-time spectrum obtained over a 21-second interval (0248:02–0248:23 UT) on August 1, 1985.

A-G90-431

PDP, AUG. 1, 1985
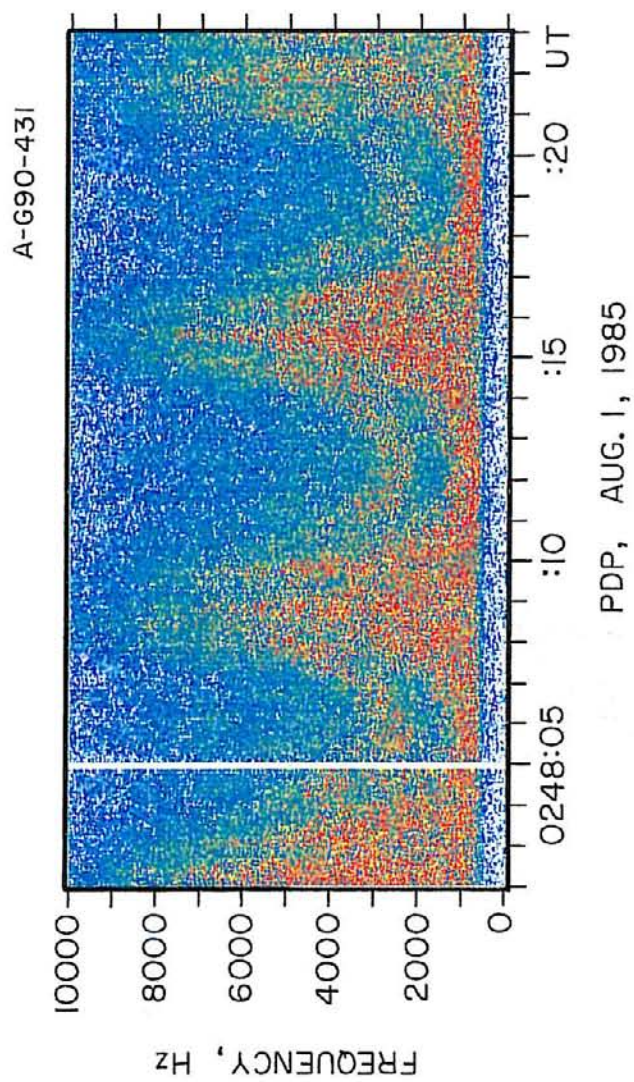
Figure 4.4: An example of a partially formed interference pattern observed in the 0–10 kHz electric field wideband spectrum. This frequency-time spectrum was obtained over a 24-second interval (0411:39–0412:03 UT) on August 1, 1985.

PDP

FREQUENCY (Hz)

BEGIN 85 213 04:11:39   END 85 213 04:12:03 GMT

PROCESSED 26-SEP-90
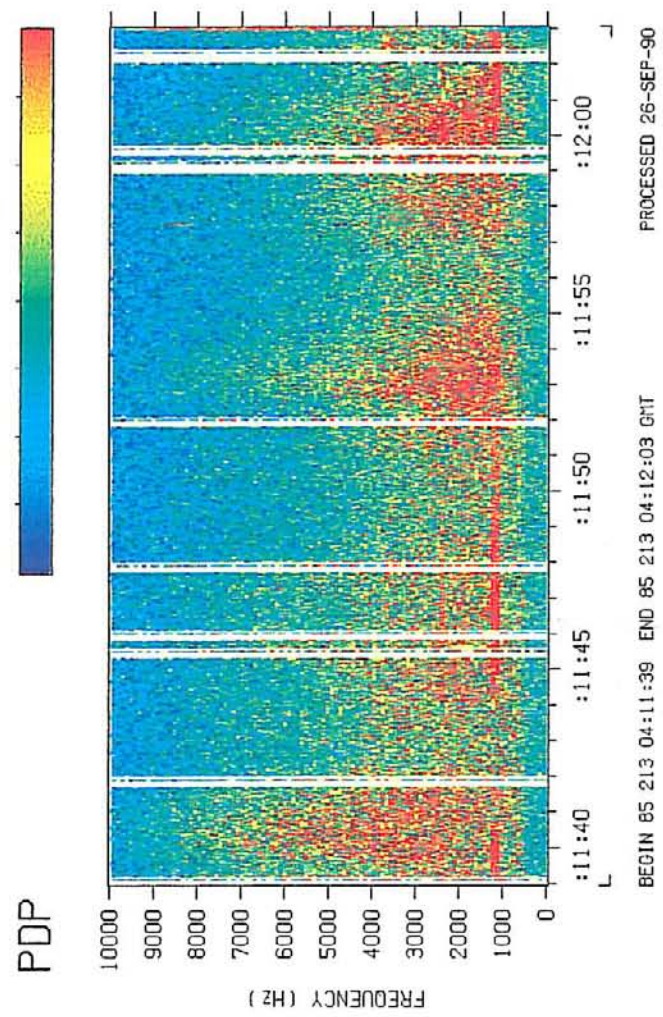
Figure 4.5: An example of an interference pattern observed in the 10–20 kHz electric field wideband spectrum. This frequency-time spectrum was obtained over a 13-second interval (0038:42–0038:55 UT) on August 1, 1985. The quantities X, Y and Z are LVLH coordinates.

A-G85-1019

FREQUENCY, kHz

0038:45   :50   :55
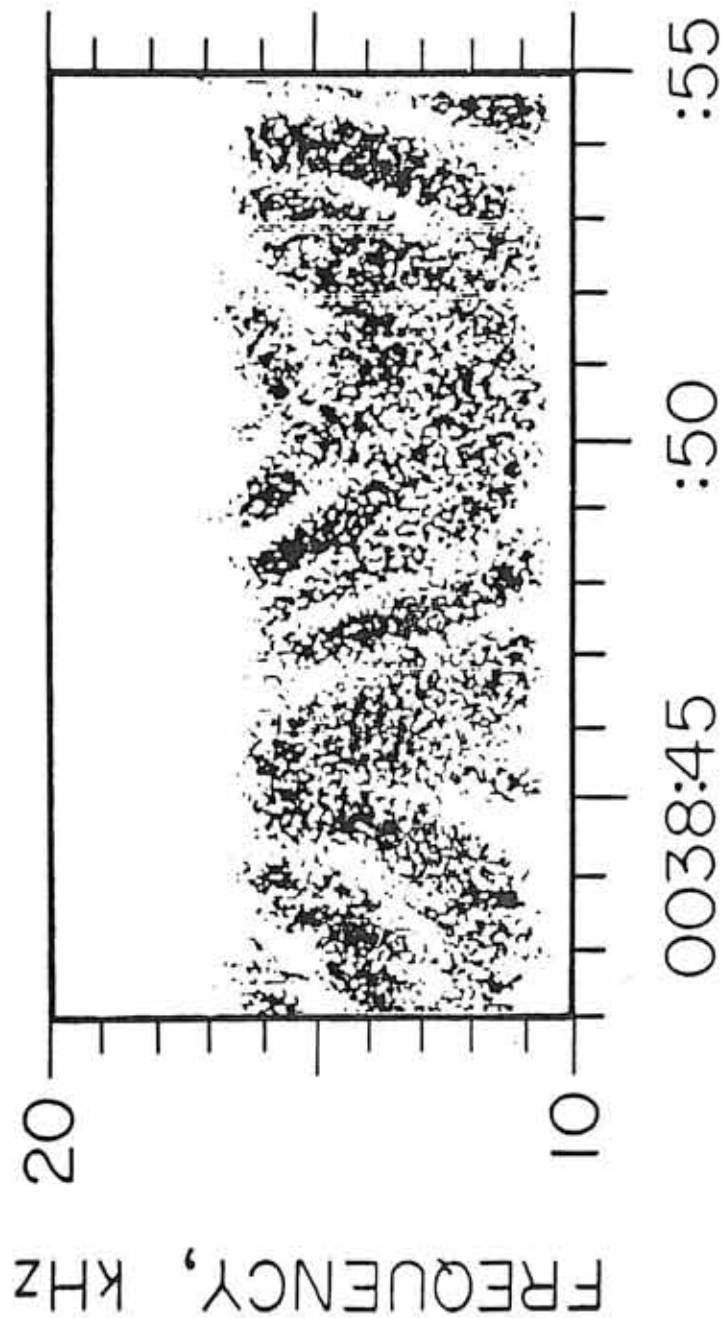
X = 87 m,   Y = 1 m,   Z = −5 m

PDP,   DAY 213,   AUG. 1, 1985

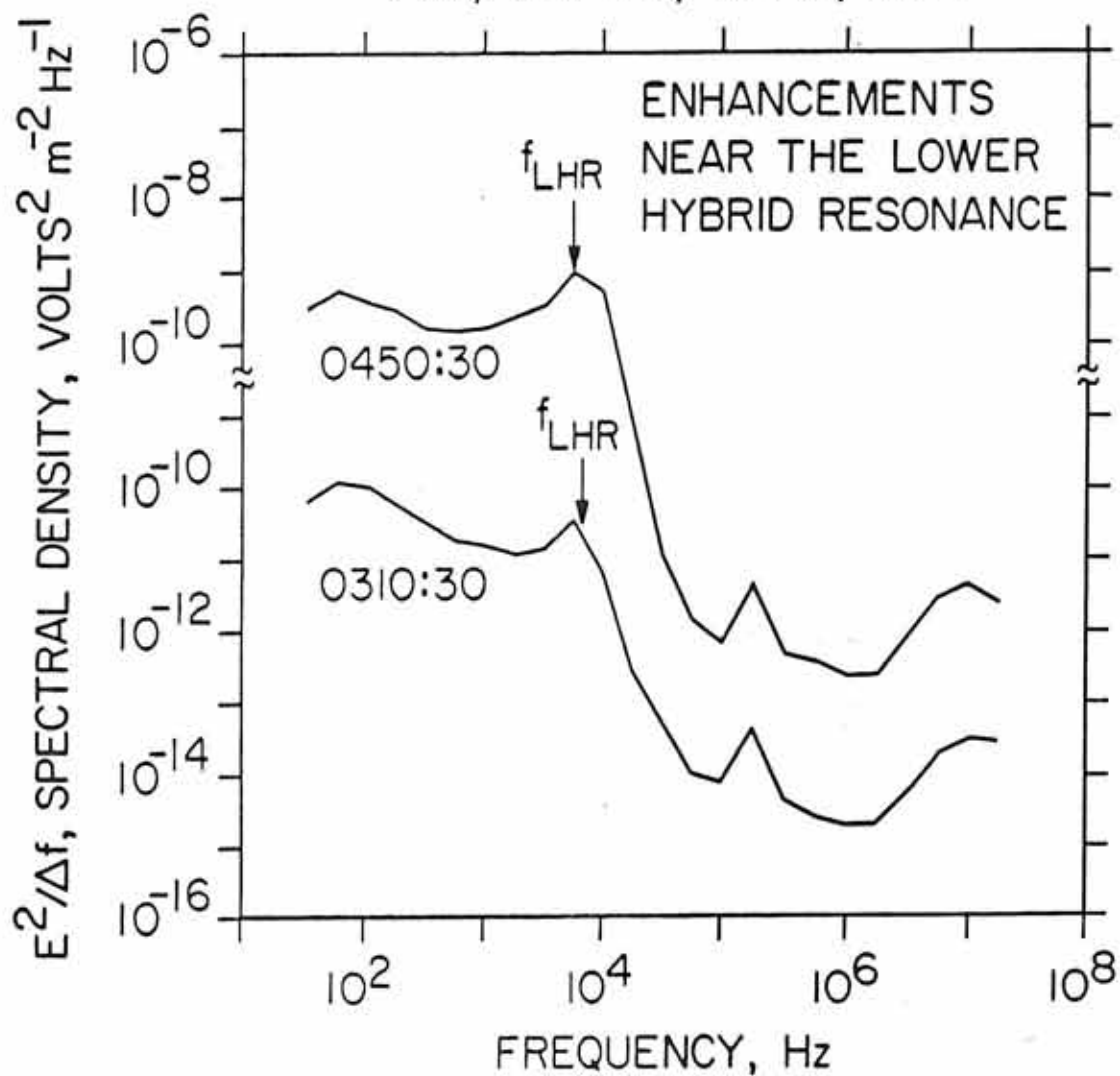Figure 4.6: An example of an interference pattern observed in the 0–10 kHz electric field wideband spectrum. This spectrum was obtained over a 25-second interval (0200:12–0200:37 UT) on August 1, 1985. The quantities X, Y and Z are LVLH coordinates.

A-G85-1018
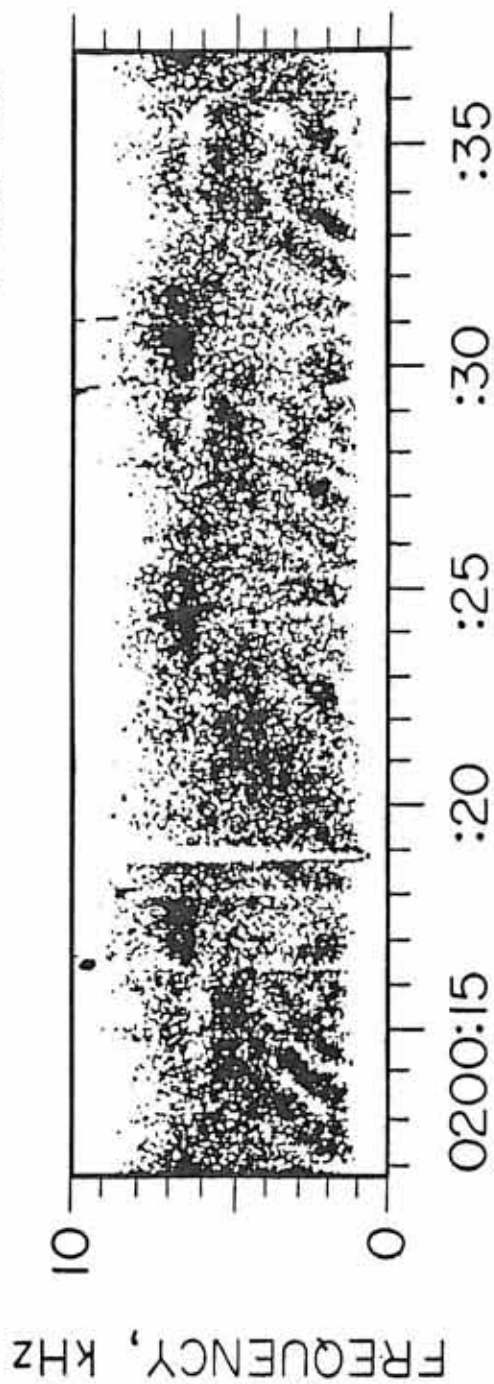
X = -20 m, Y = 26 m, Z = -200 m

PDP, DAY 213, AUG. 1, 1985

Figure 4.7: Wavevector directions of the lower hybrid waves and the
corresponding directions of the Earth's magnetic field plotted on
the PDP trajectory around the shuttle during the period 0124–0441 UT.

PDP TRAJECTORY RELATIVE TO THE SHUTTLE
01:24 – 04:41 UT

EARTH

PDP TRAJECTORY

SHUTTLE

$\overline{K}$

$\overline{B}$

○ EVERY MINUTE

□ EVERY 5 MINUTES

X_{LVLH} (M)

Z_{LVLH} (M)

-300   -200   -100   0   100   200   300

200   100   0   -100   -200
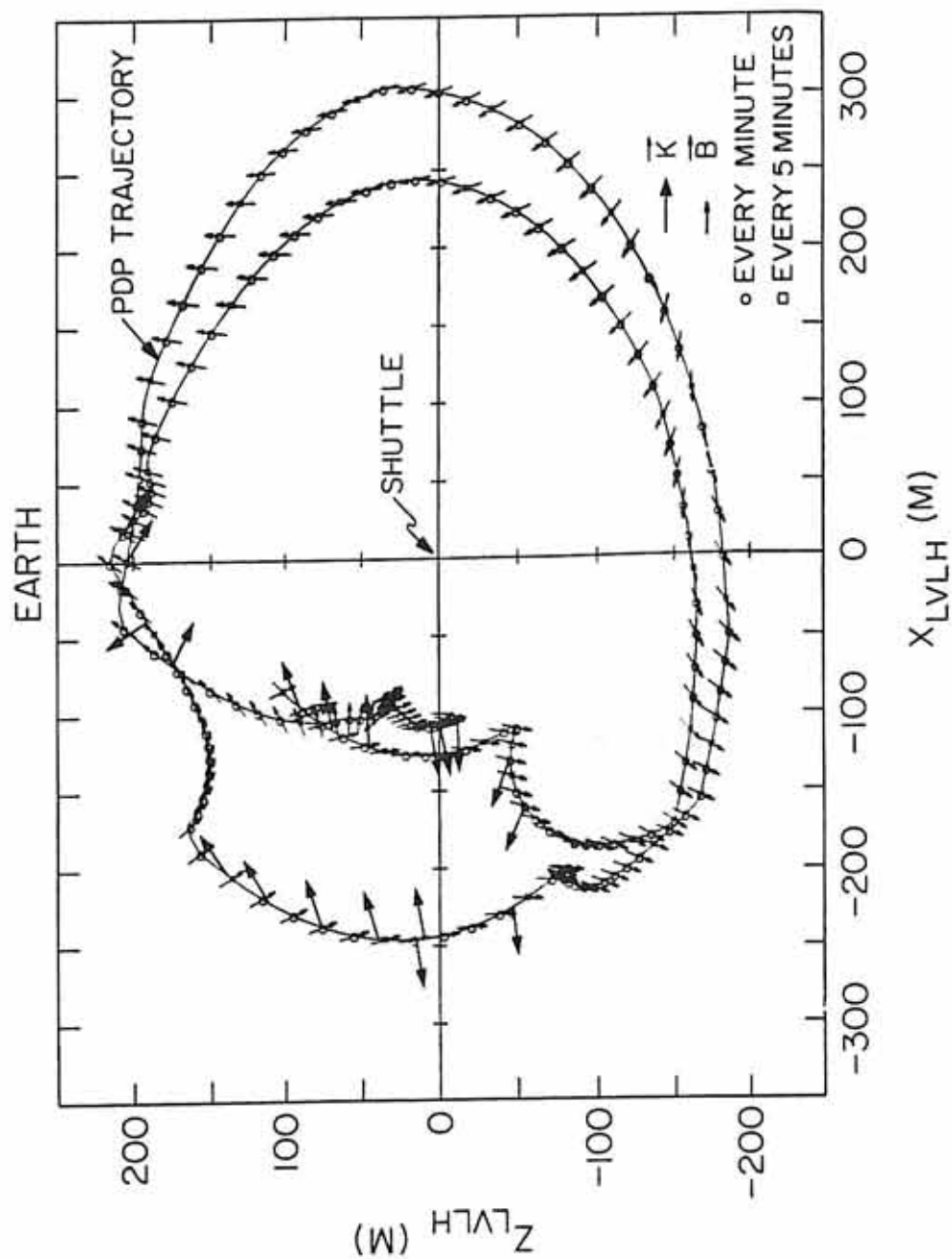
Figure 4.8: The electric field spectral density as a function of frequency during the 0310 UT and 0450 UT events. There are clear enhancements near the lower hybrid resonance frequency.

A-G87-251

PDP, DAY 213, AUG. 1, 1985

Figure 4.9: A "tilted" interference pattern observed in the 0–10 kHz electric field wideband spectrum. This spectrum was obtained over a 20-second interval (0310:15–0310:30 UT) on August 1, 1985.

A-G92-316

FREQUENCY, kHz

0310:20 :30
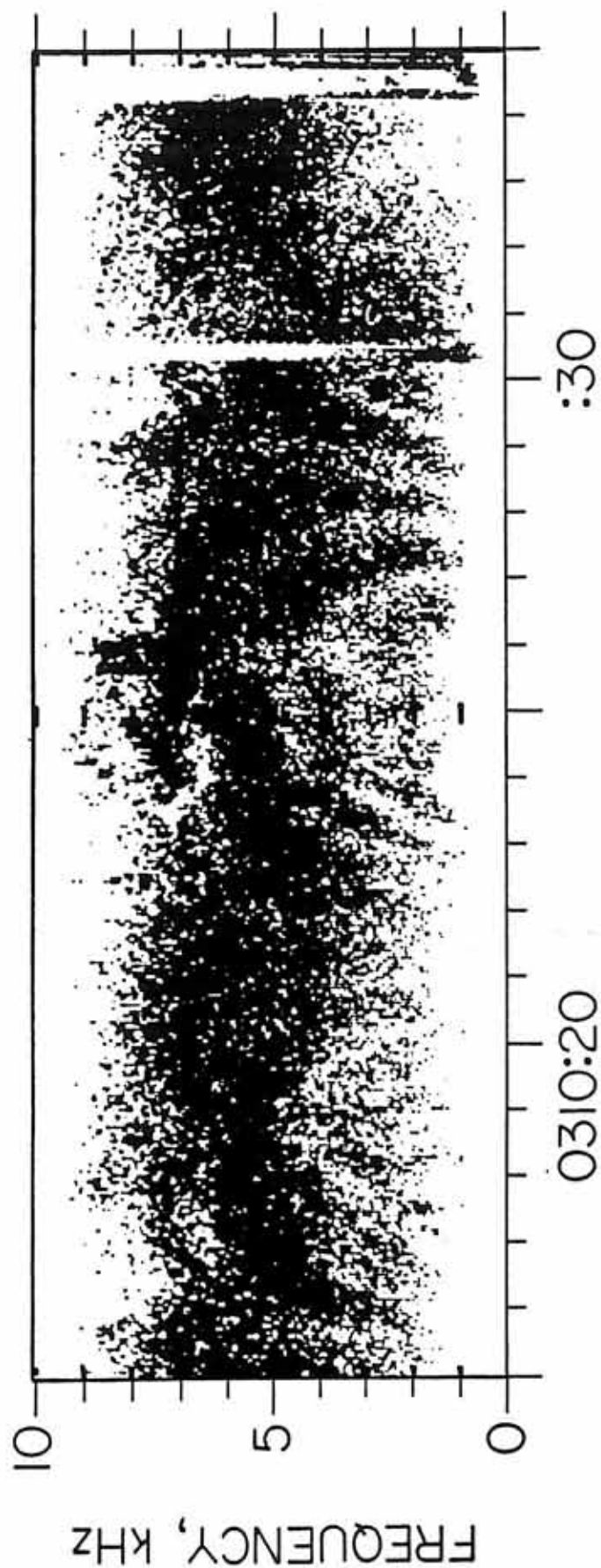
X = 198 m, Y = -19 m, Z = -145 m

PDP, DAY 213, AUG. 1, 1985

87

Figure 5.1: A snapshot electric field power spectrum obtained at 0046:57.6–0046:58.0 UT. A least squares fit was used to determined the maxima and null position of the interference pattern for the 0046–0047 UT event.

LEAST SQUARES FIT
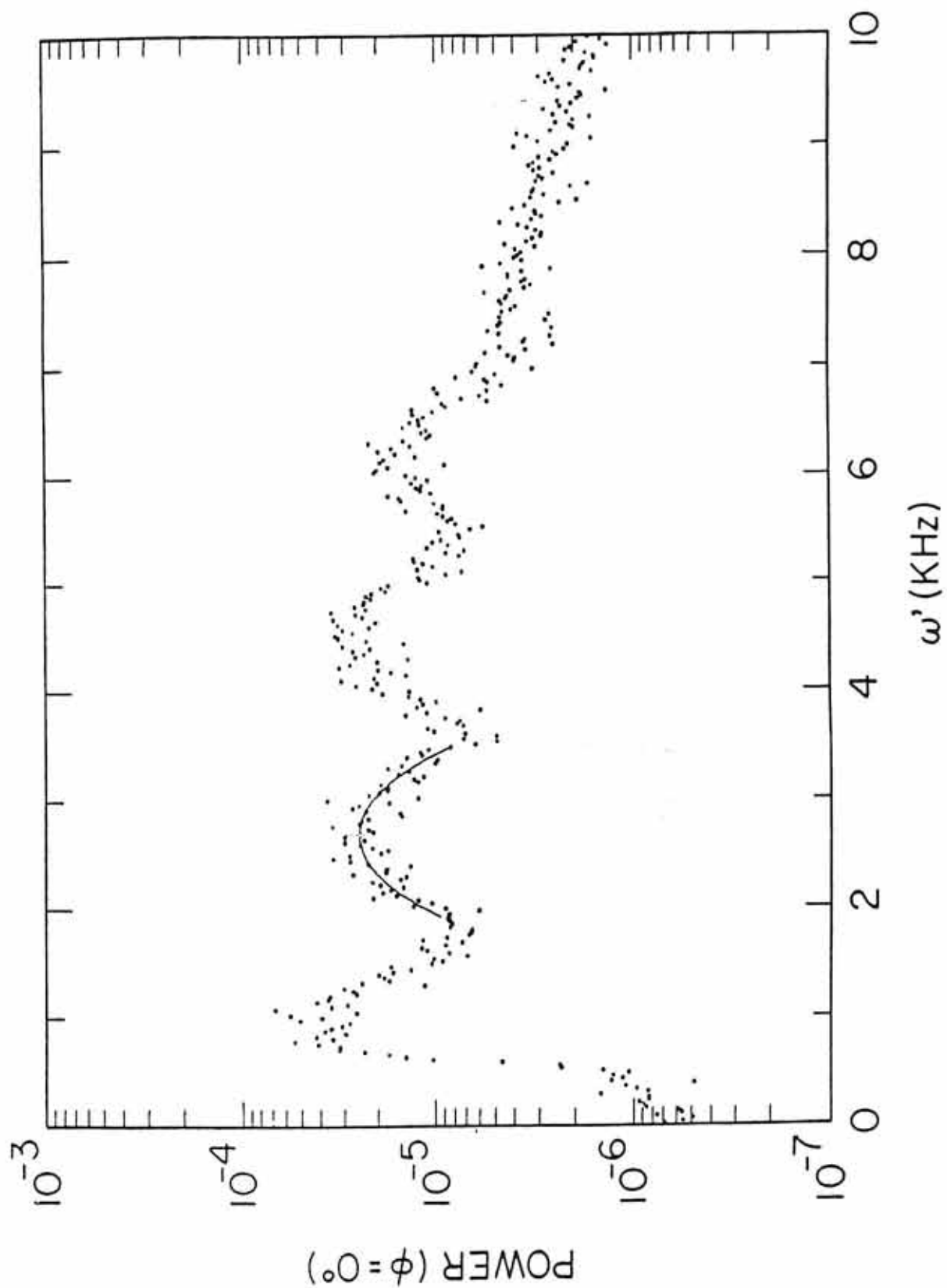
B-G90-440

Figure 5.2: The dispersion relation of the electrostatic low frequency waves in the 2-D X-Z plane for the 0046–0047 UT event. The label ω_0 is the wave frequency in the plasma rest frame. The errors are about ± 0.1 kHz.

DISPERSION RELATION IN 2-D X-Z PLANE

B-G90-441

INTEGRATED TIME INTERVAL

□	400 MSEC
+	666 MSEC
*	800 MSEC
○	1200 MSEC
×	2000 MSEC
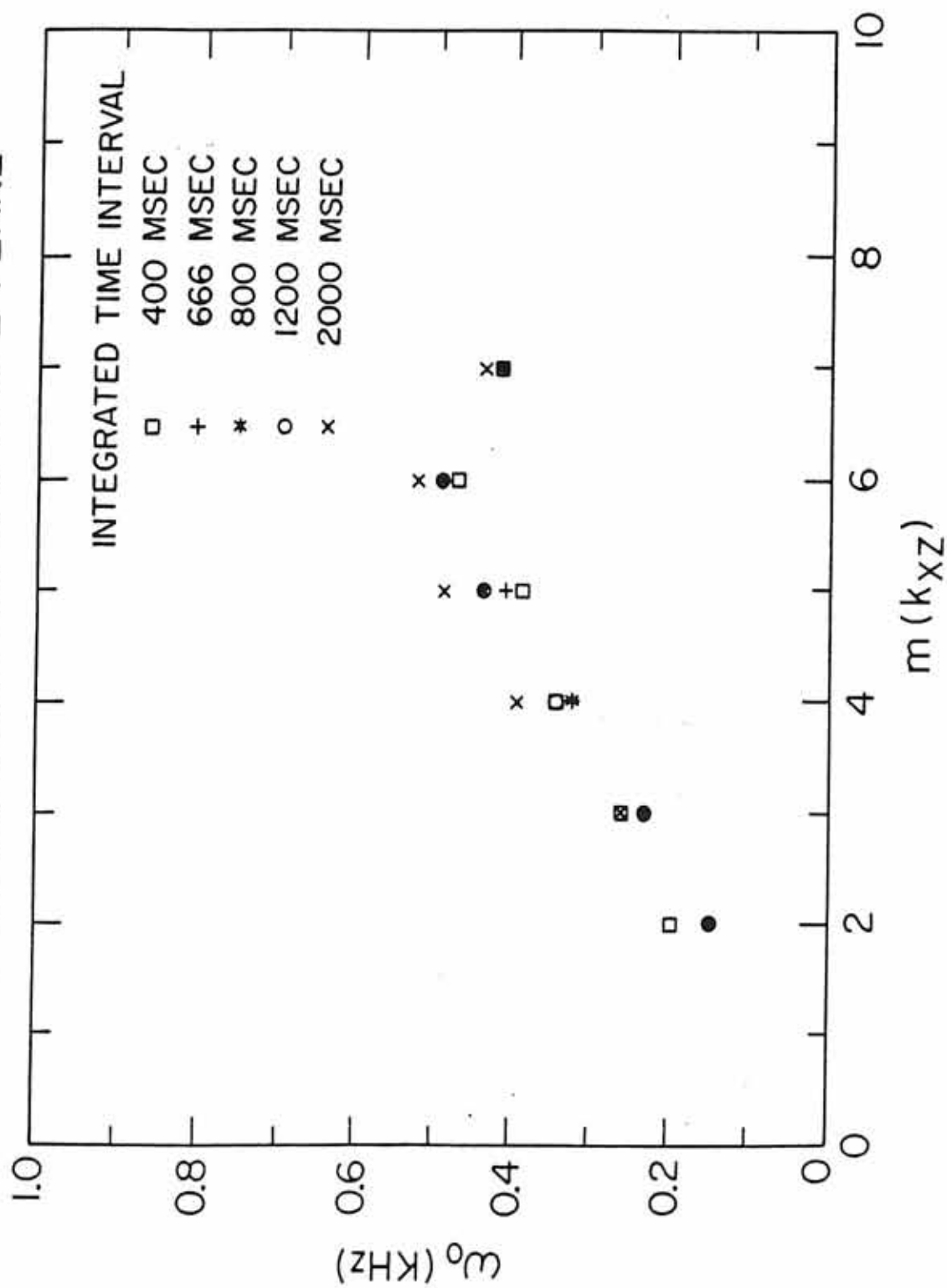
Figure 5.3: Inferred true power spectrum obtained from the measured power spectrum by eliminating antenna interference effects.

A-G9I-476

POWER DENSITY SPECTRUM
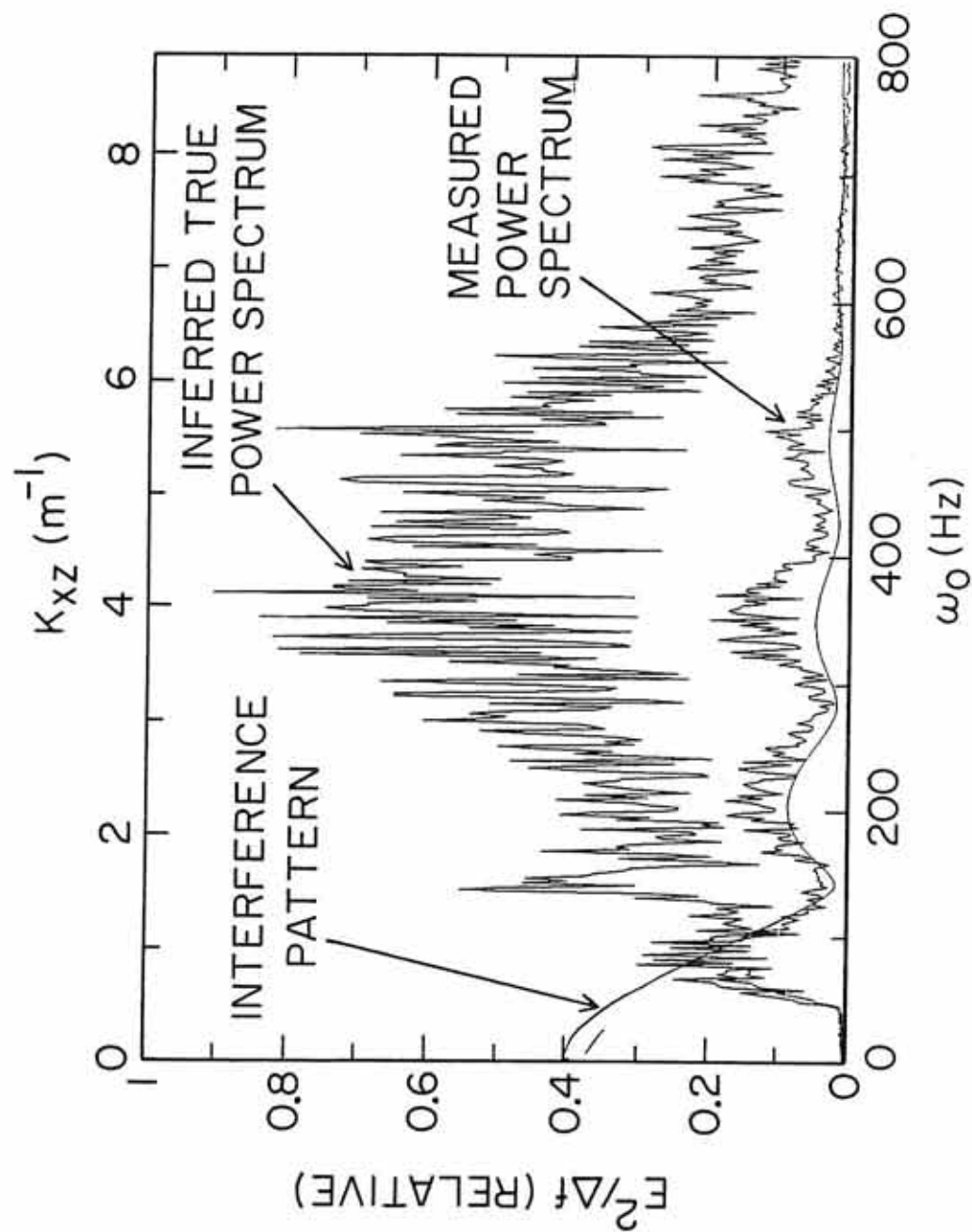
Figure 5.4: The PDP and the wave source position for the 0046-0047 UT event projected onto the X-Z plane.

A-G90-445-3

0046 UT

Figure 5.5: The PDP and the wave source position for the 0247-0050 UT event projected onto the X-Z plane.
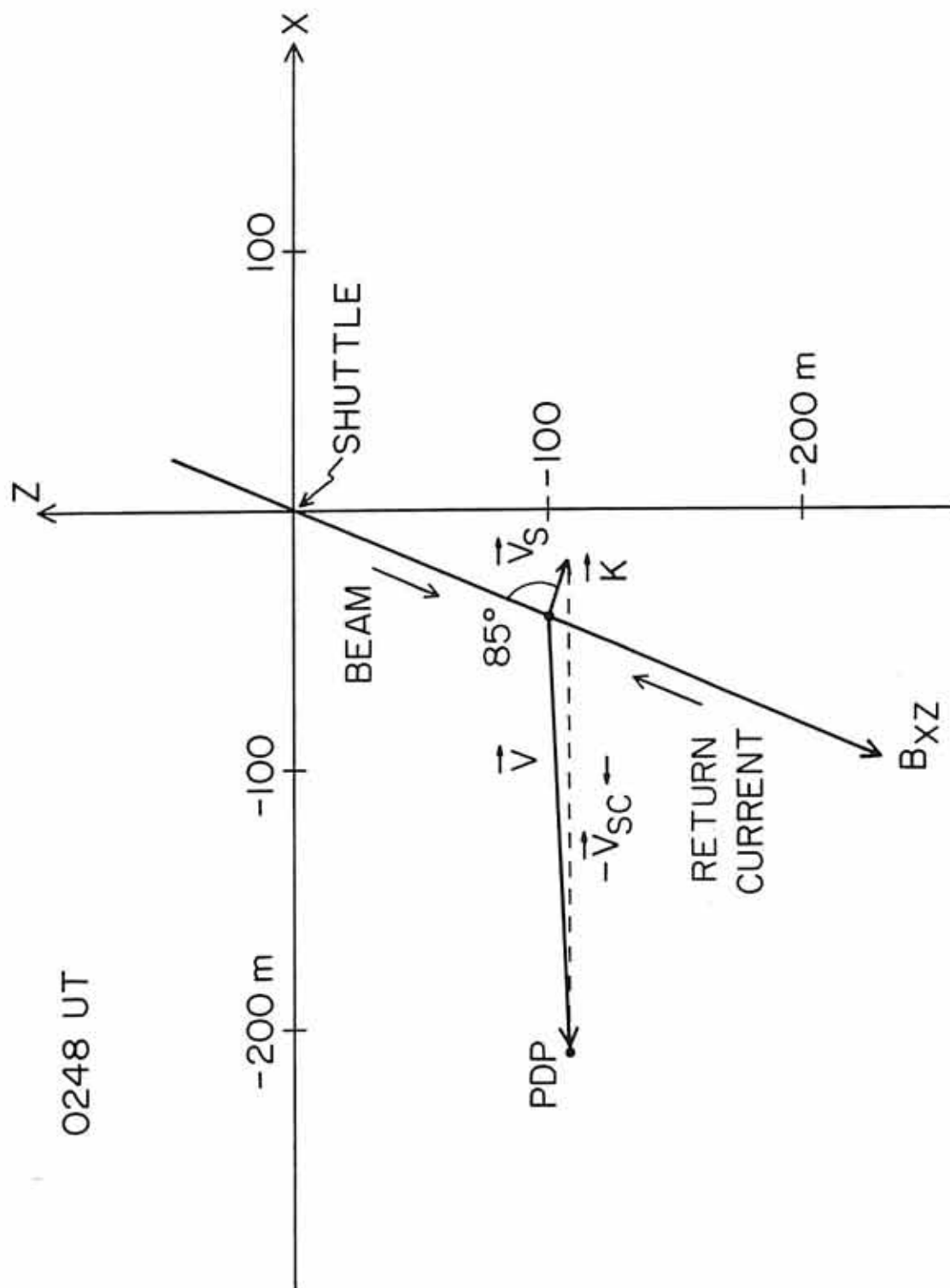
Figure 5.6: The PDP and the wave source position for the 0247-0250 UT event projected onto the Y-Z plane. The circle is the region within which waves can be generated and subsequently observed by the PDP.
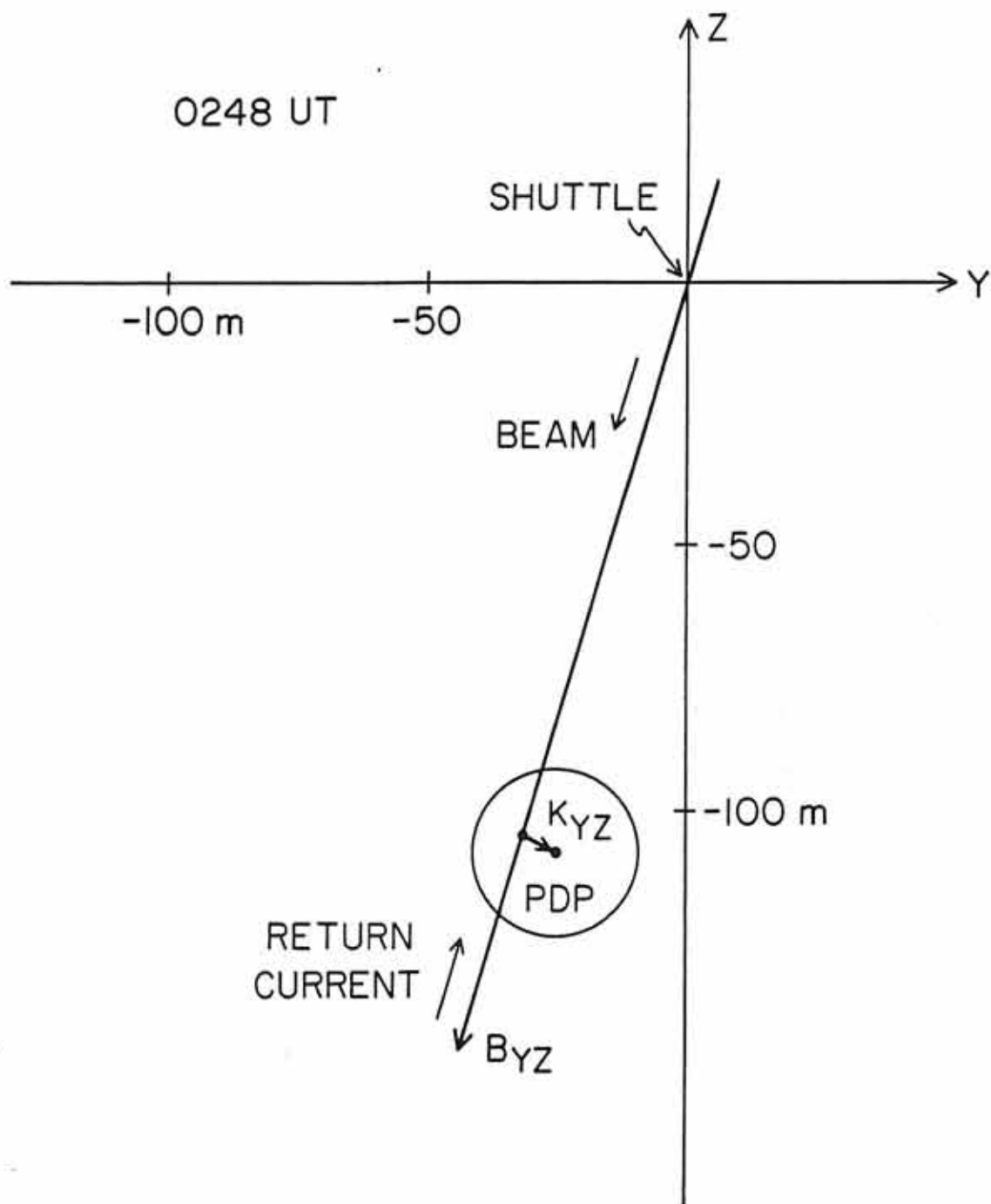
Figure 5.7: Theoretical interference patterns for a Gaussian angular distribution of waves. Assuming the range of wave-propagating angles θ is two standard deviations: (a): $\theta = 0°$, (b): $\theta = 5°$, (c): $\theta = 10°$, (d): $\theta = 15°$.
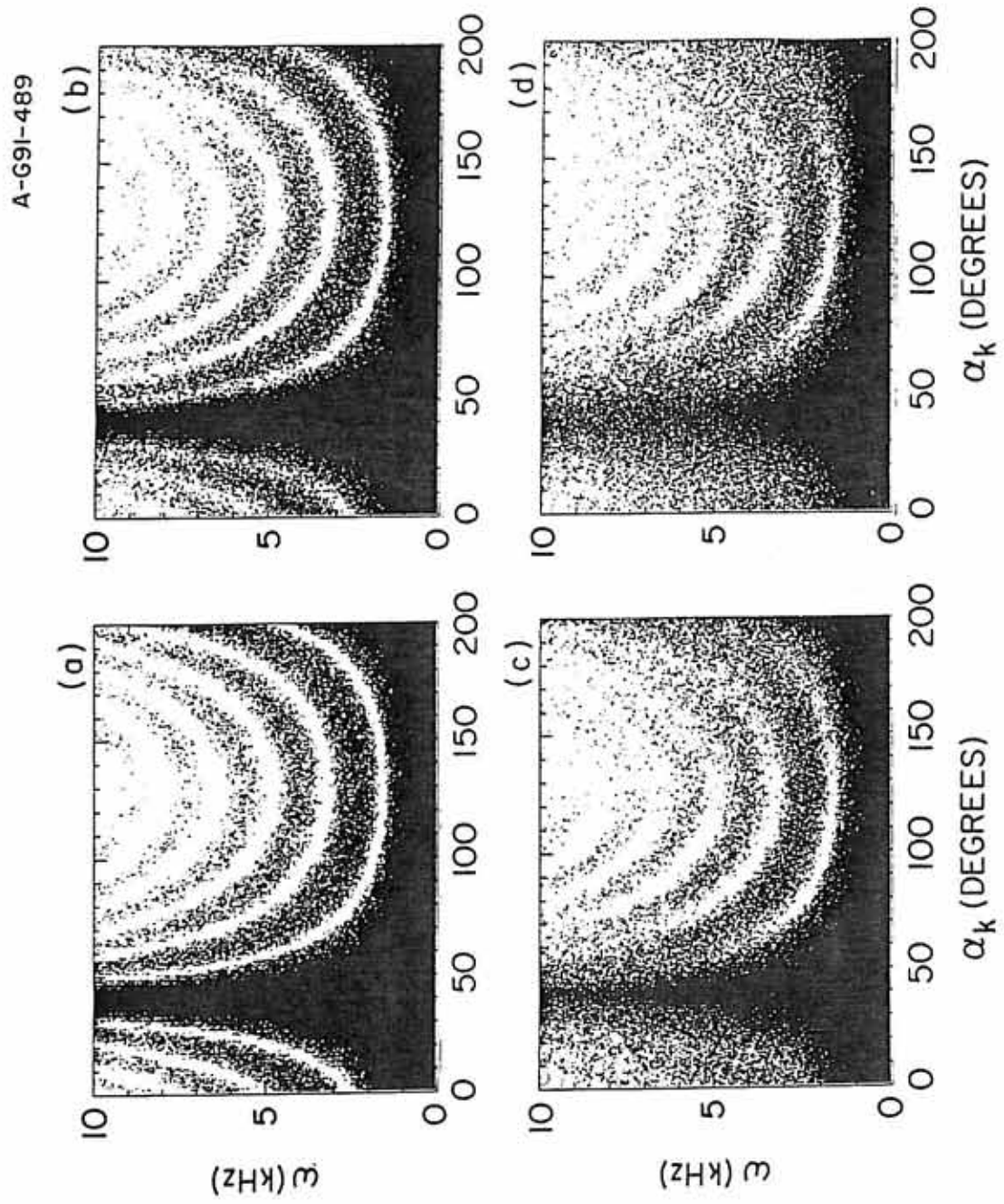
Figure 5.8: Maximum wave growth rates as a function of the wave propagation angle relative to the magnetic field. Parts (a)-(d) correspond to different drift speeds V_e for the ambient electrons. (a). $V_e/V_{te} = 0.60$. (b) $V_e/V_{te} = 0.72$. (c) $V_e/V_{te} = 0.80$. (d) $V_e/V_{te} = 1.0$.
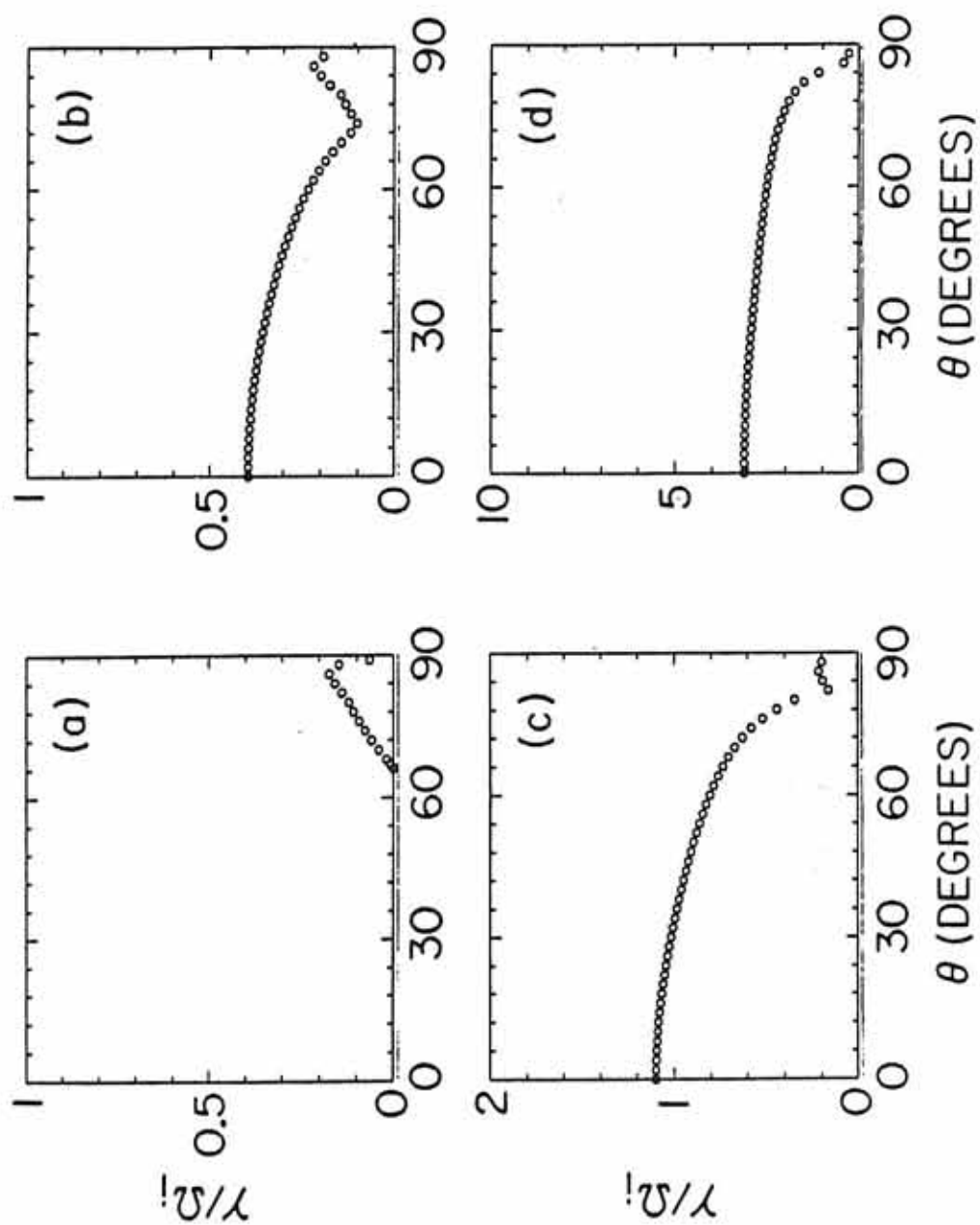
Figure 5.9: Linear dispersion relation (filled circles) and growth rate (open circles) of the oblique ion acoustic-like waves with $\theta = 86.5°$ and $V_e = 1.0V_{te}$. The remnants of ion cyclotron-like structures are visible at small wavenumbers. The order of the ion cyclotron harmonics is labeled by M.
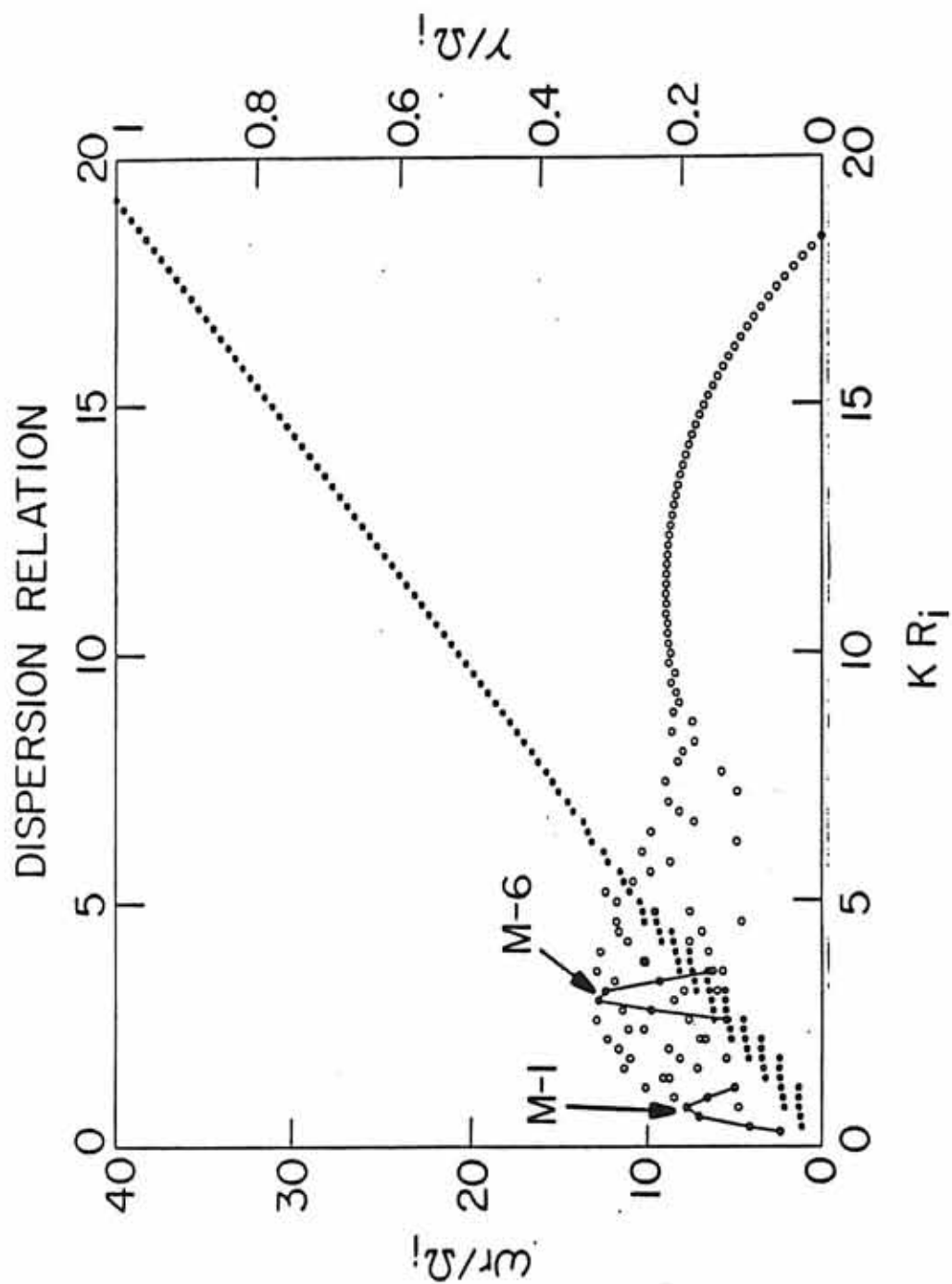
DISPERSION RELATION

A-G9I-604

Figure 6.1: Dispersion relation in the 2-D X-Z plane for the 0038 UT

event. The thin line is the cold plasma dispersion relation of lower

hybrid waves (Appendix). The thick dashed line is the lower hybrid

frequency. The errors are about ± 0.2 kHz.

B-G92-320-1

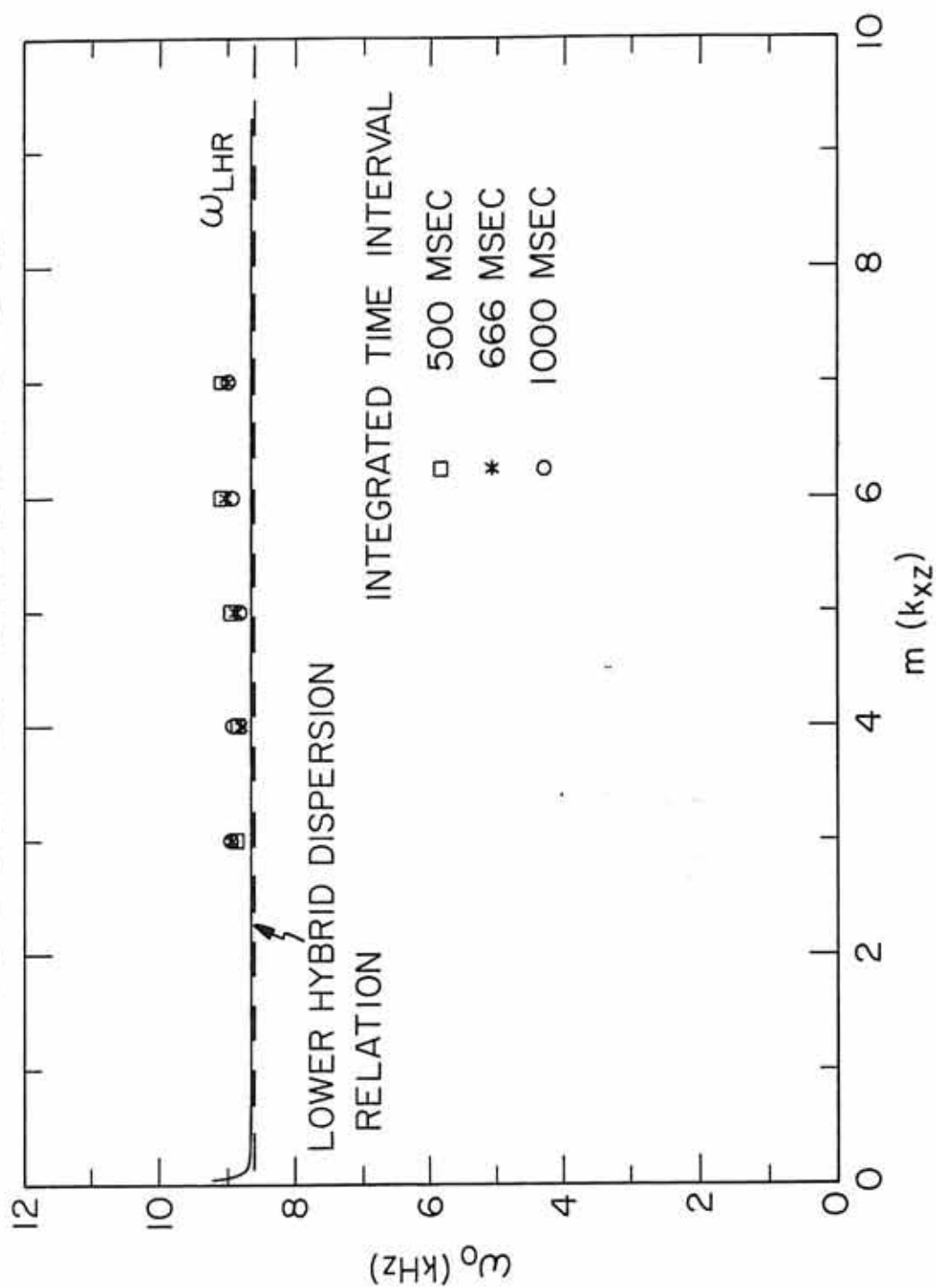DISPERSION RELATION IN 2-D X-Z PLANE

Figure 6.2: Power density spectra for the 0038 UT event.
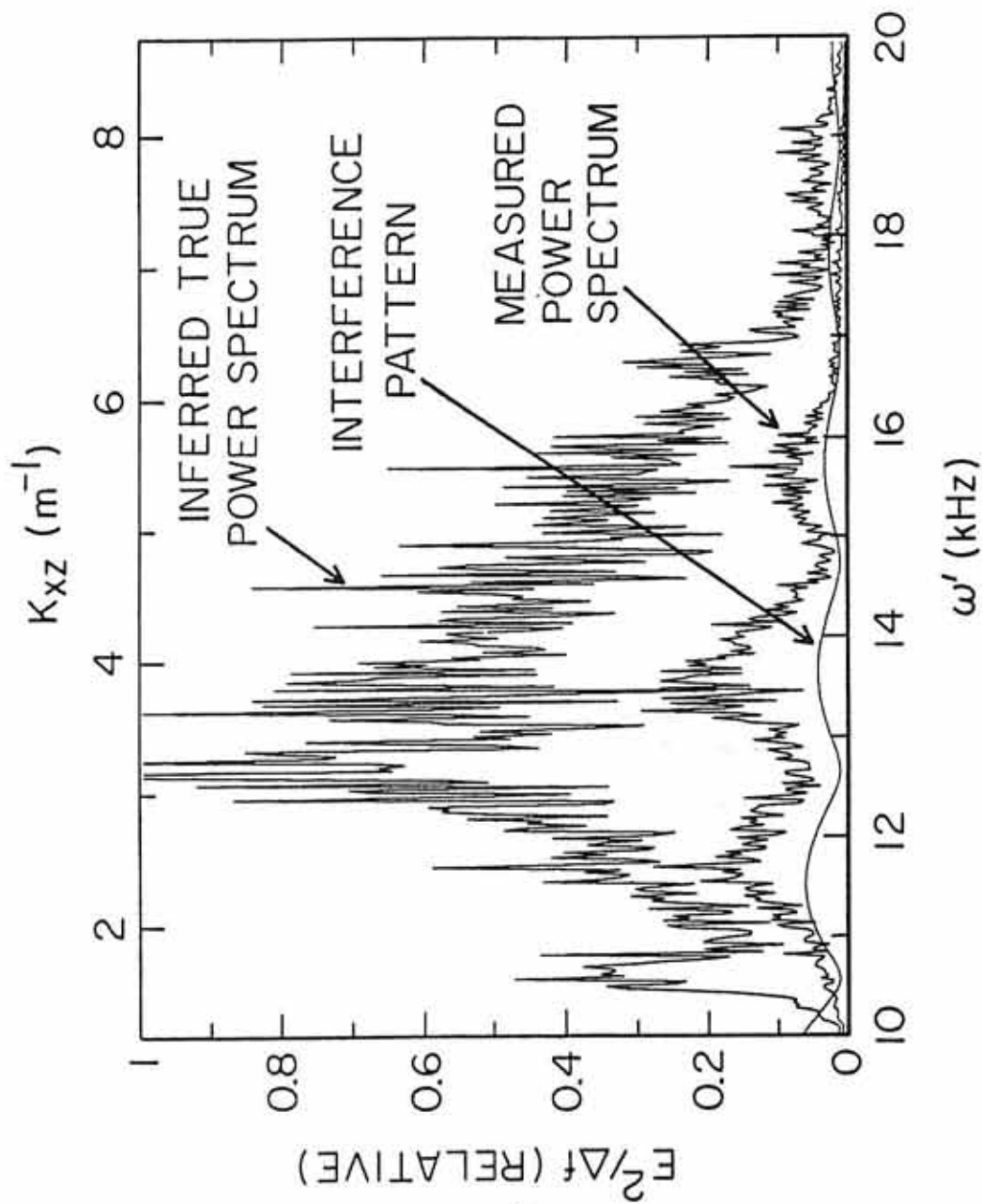
POWER SPECTRUM 0038:43 UT

A-G92-318

Figure 6.3: Simulation of a "tilted" interference pattern, assuming that α_{k0} varies linearly with wavenumber k_{xz}.

SIMULATED "TILTED" INTERFERENCE PATTERN

A-G92-319-1
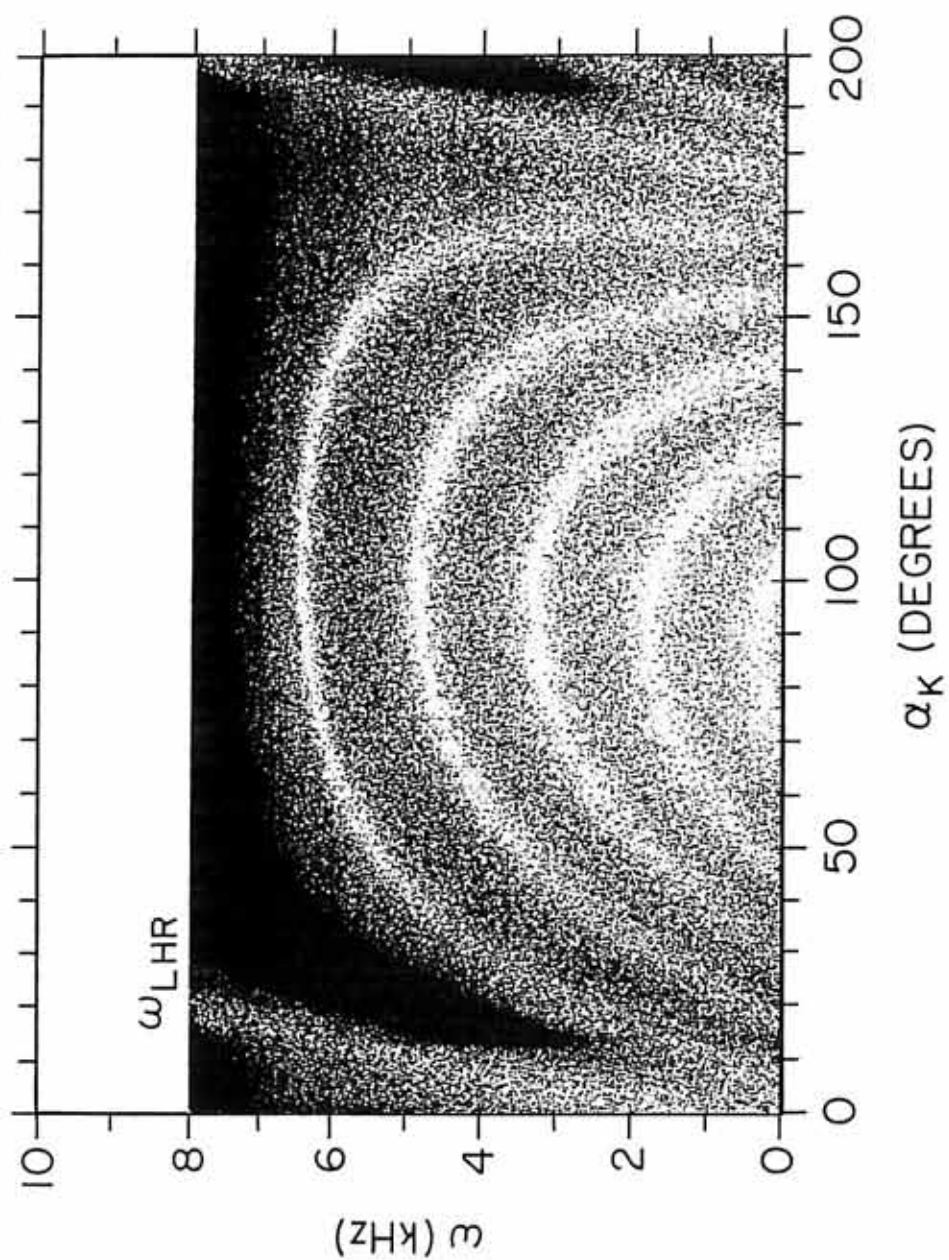
ω_{LHR}

ω (kHz)

α_K (DEGREES)

Figure 6.4: A broadband electric field spectrogram from the Helios and MFR data for the time period 0312–0336 UT, August 1, 1985.
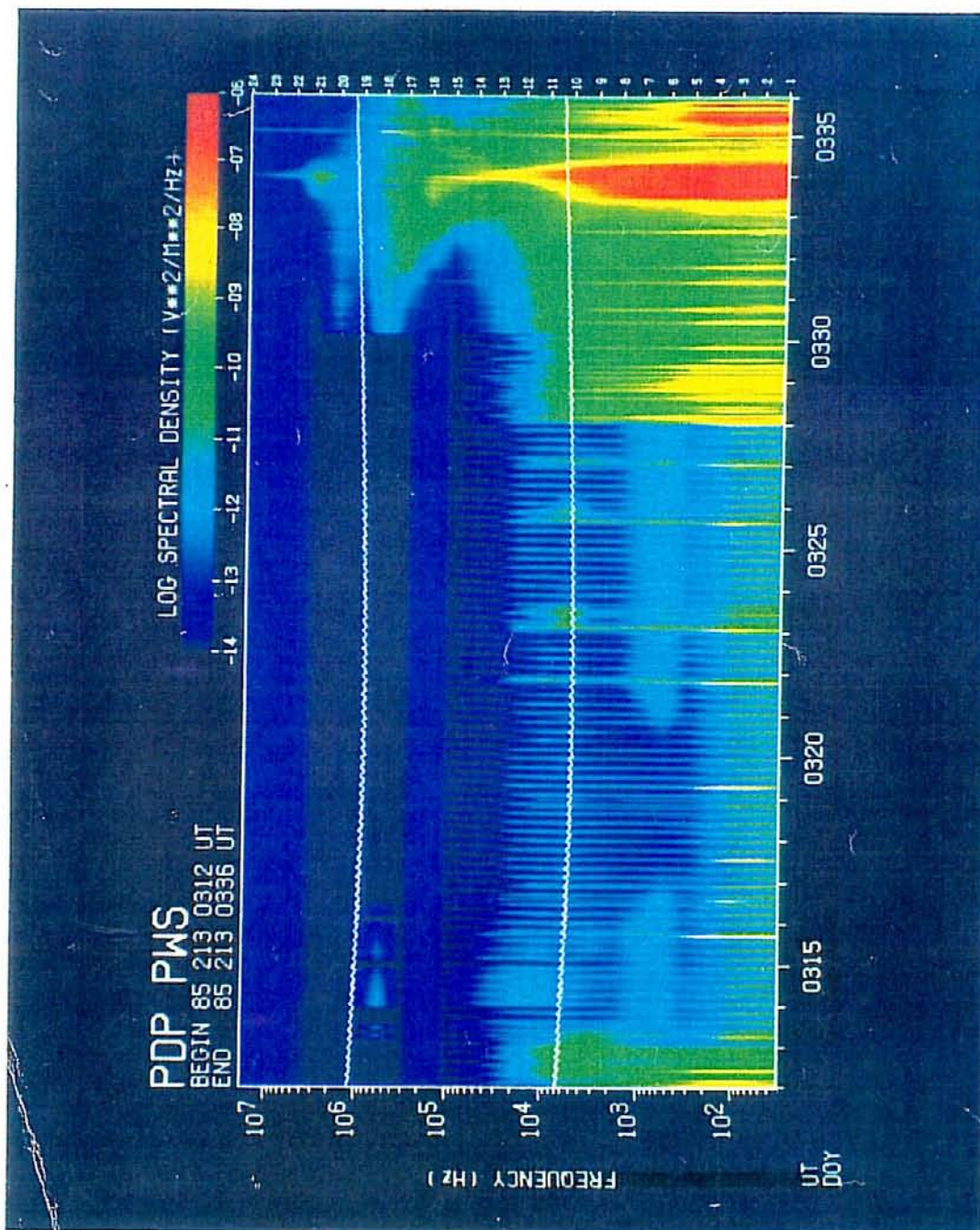
Figure 6.5: An idealized "mushroom" spectral feature copied from Cairns and Gurnett [1991]. This spectrum is plotted on a semi-log scale.
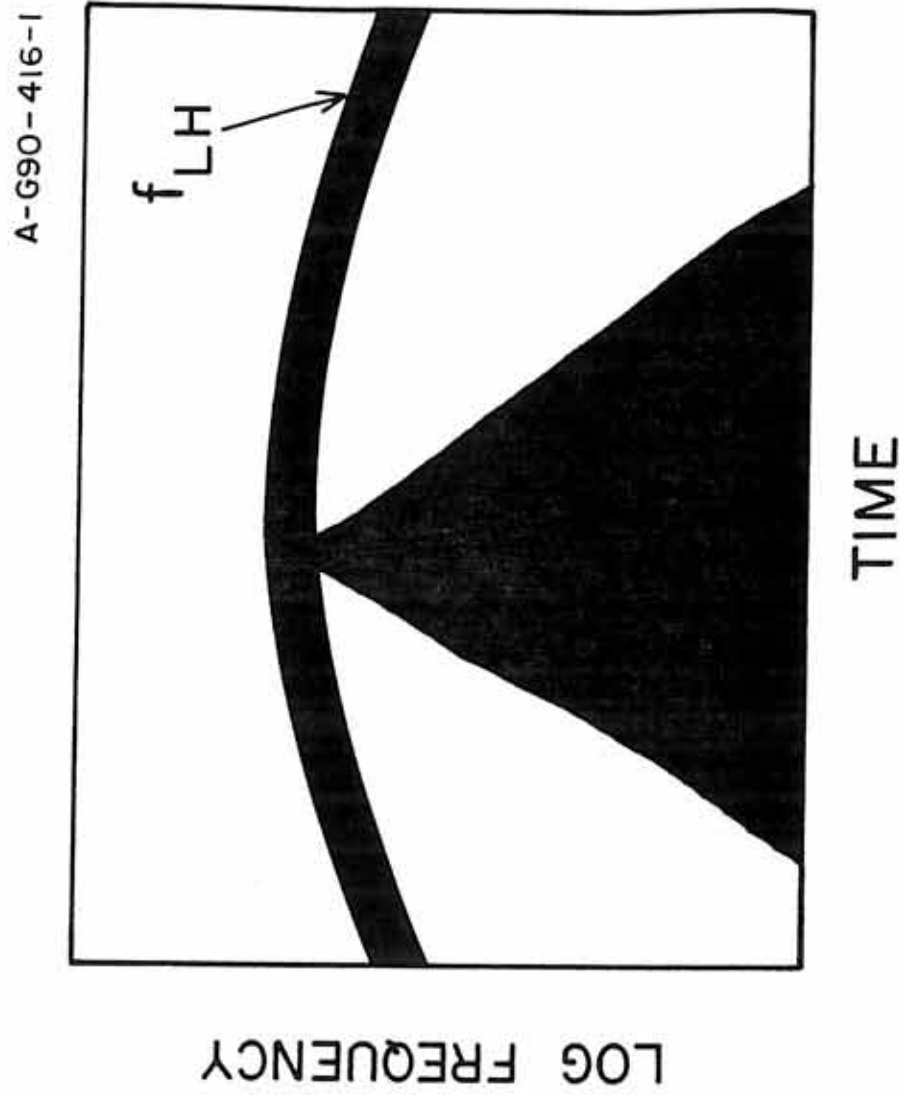
Figure 6.6: Comparison of the relative electric field spectra for the near

zone and free flight waves. The dashed line is the average spectra

for the near zone waves during the period 0145–0210 UT on Day 212,

1985. The solid line is the free flight spectra measured at the

center of the "mushroom" during the period 0304:45–0305:45 UT on

Day 213, 1985.

A-G92-481

PDP RELATIVE ELECTRIC FIELDS

SL-2 PDP PLASMA WAVE INSTRUMENT

——, FREE-FLIGHT
85 213 0304:45-0305:45 UT

––––, NEAR ZONE
85 212 0145-0210 UT

Figure 6.7: Comparison of the average electric field spectral density as a function of frequency for the near zone and free flight waves. The dashed line shows the near zone spectra during the period 0145–0210 UT on Day 212, 1985. The solid line is the free flight spectra measured at the center of the "mushroom" during the period 0304:45–0305:45 UT on Day 213, 1985.
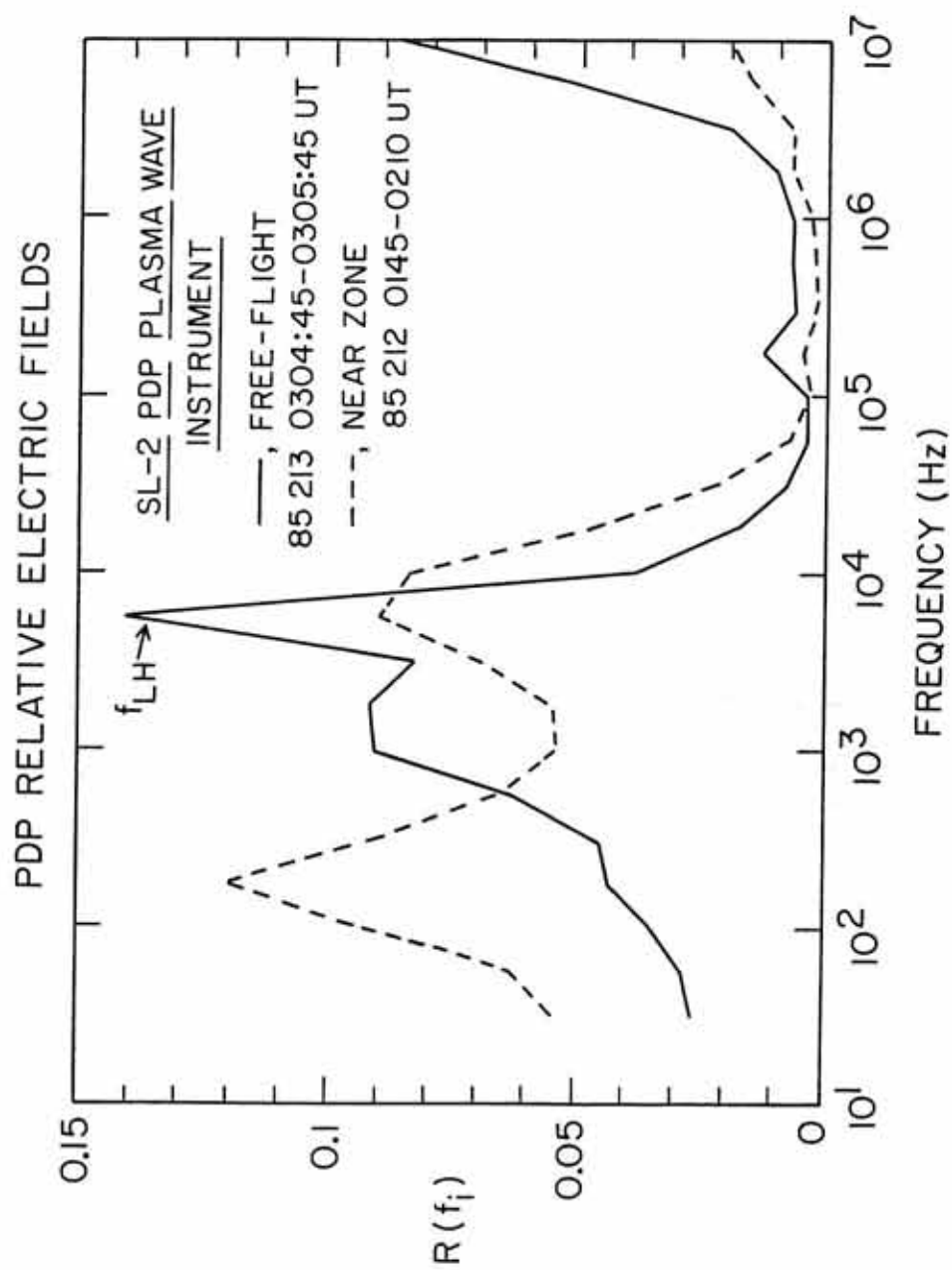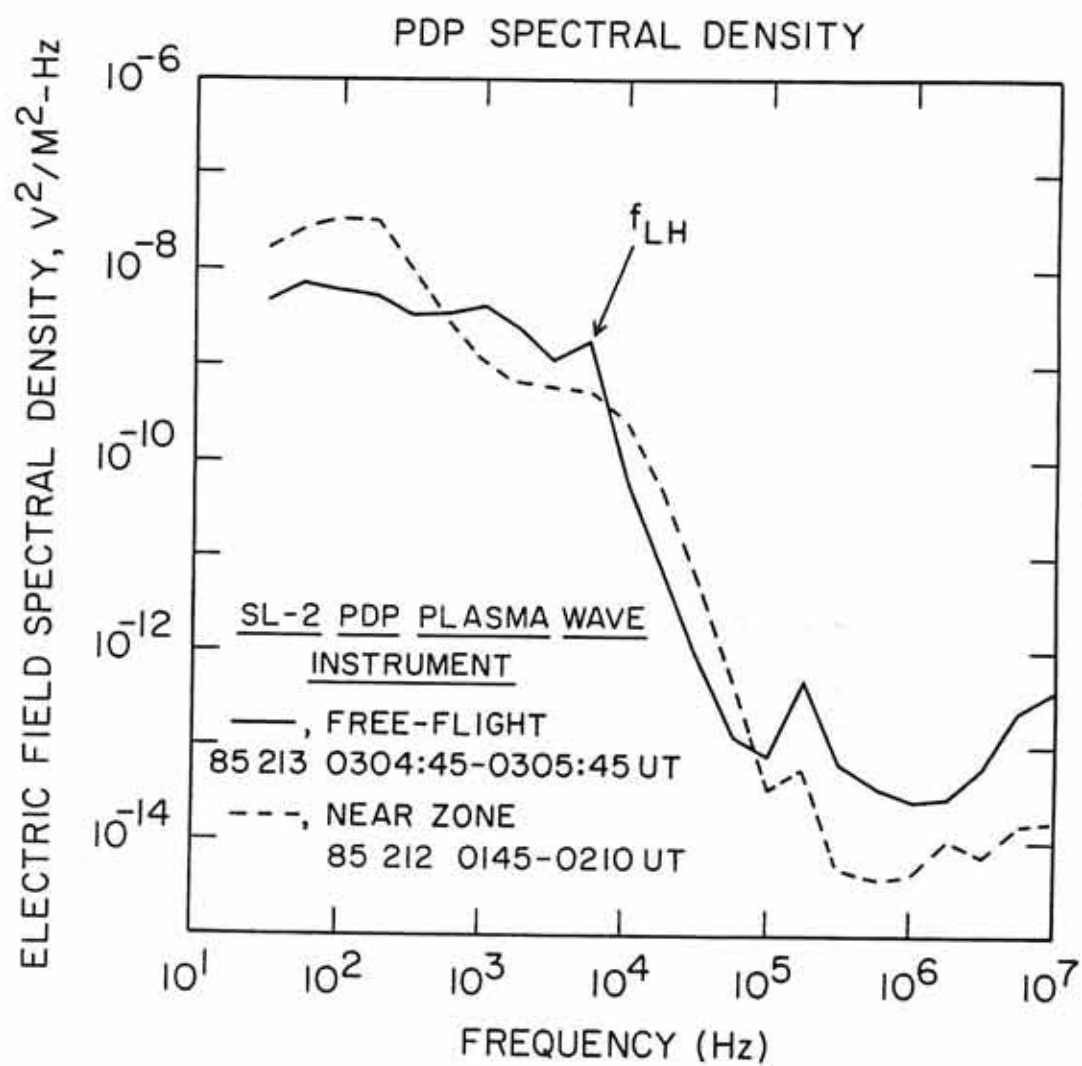
A-G92-482

PDP SPECTRAL DENSITY

APPENDIX:

COLD PLASMA DISPERSION RELATION OF LOWER HYBRID WAVES

This appendix is referred to Chapter VI, where interference patterns associated with the lower hybrid waves are discussed. A cold plasma dispersion relation is needed to compare with the measured dispersion relation of lower hybrid waves.

Let us define a dimensionless index of refraction

$$N = \frac{kc}{\omega}$$

The dispersion equation of waves in a cold plasma [Miyamoto, 1989] is

$$AN^4 - BN^2 + C = 0,$$

where

$$A = K_\perp sin^2\theta + K_\parallel cos^2\theta$$

$$B = (K_\perp^2 - K_x^2)sin^2\theta + K_\parallel K_\perp(1 + cos^2\theta)$$

$$C = K_\parallel(K_\perp^2 - K_x^2).$$

Here θ is the angle between the wavevector and the magnetic field. The dielectric tensor components are defined by

$$K_\perp = 1 - \sum_k \frac{\omega_{pk}^2}{\omega^2 - \Omega_{ck}^2}$$

$$K_x = \sum_k \frac{\omega_{pk}^2}{\omega^2 - \Omega_{ck}^2} \left(\frac{\Omega_{ck}}{\omega} \right)$$

$$K_{\parallel} = 1 - \sum_k \frac{\omega_{pk}^2}{\omega^2}.$$

For waves propagating (almost) perpendicular to the magnetic field ($\theta \cong \pi/2$), the dispersion equation is given by

$$K_{\perp} N^4 - (K_{\perp}^2 - K_x^2 + K_{\parallel} K_{\perp}) N^2 + K_{\parallel}(K_{\perp}^2 - K_x^2) = 0.$$

The solution for lower hybrid waves is

$$N^2 = \frac{K_{\perp}^2 - K_x^2}{K_{\perp}}.$$

Therefore, the dispersion relation is

$$k = \frac{\omega}{c} \sqrt{\frac{K_{\perp}^2 - K_x^2}{K_{\perp}}}.$$

Let us consider only two species: electrons and oxygen ions. For waves near the lower hybrid frequency under the Spacelab 2 condition, the two conditions, $\omega_{pe}^2 \gg \Omega_{ce}^2$ and $\omega \sim \omega_{LHR}$, lead to

$$K_{\perp} \cong 1 - \frac{\omega_{pi}^2}{\omega^2} + \frac{\omega_{pe}^2}{\Omega_{ce}^2}$$

$$K_x \cong \frac{\omega_{pe}^2}{\Omega_{ce}\omega}.$$

The thin line in Figure 6.1 is produced according to the above dispersion relation.

REFERENCES

Buneman, O., Instability, turbulence, and conductivity in a current carrying plasma, Phys. Rev. Lett., 1, 8, 1958.

Bush, R. I., G. D. Reeves, P. M. banks, T. Neubert, P. R. Williamson, W. J. Raitt, and D. A. Gurnett, Electromagnetic field from Pulsed Electron Beam experiment in space: Spacelab-2 results, Geophys. Res. Lett., 14, 1015, 1987.

Cai, D., T. Neubert, L. R. Storey, P. M. Banks, S. Sasaki, K. Abe, and J. L. Burch, ELF oscillations associated with electron beam injection from the space shuttle, J. Geophys. Res., 92, 12451, 1987.

Cairns, I. H., Transition from ring to beam arc distribution of water ions near the space shuttle orbiter, J. Geophys. Res., 95, 15167, 1990.

Cairns, I. H. and D. A. Gurnett, Control of plasma waves associated with the space shuttle by the angle between the orbiter's velocity and the magnetic field, J. Geophys. Res., 96, 7591, 1991a.

Cairns, I. H. and D. A. Gurnett, Plasma waves observed in the near vicinity of the space shuttle, J. Geophys. Res., 96, 13913, 1991b.

Farrell, W. M. and Gurnett, D. A., An Analysis of Whistler Mode Radiation From the Spacelab 2 Electron Beam, J. Geophys. Res., 93, 153, 1988.

Feng, W., D. A. Gurnett, and I. H. Cairns, Interference patterns in the spacelab 2 plasma wave data: oblique electrostatic waves generated by the electron beam, J. Geophys. Res., 97, 17005, 1992.

Feng, W., D. A. Gurnett, and I. H. Cairns, Lower hybrid wave in wideband spectra in the Spacelab 2 plasma wave data, J. Geophys. Res., to be submitted, 1992.

Frank, L. A., W. R. Paterson, M. Ashour-Abdalla, D. Schriver, W. S. Kurth, D. A. Gurnett, N. Omidi, P. M. Banks, R. I. Bush, and W. J. Raitt, Electron velocity distributions and plasma waves associated with the injection of

an electron beam into the ionosphere, J. Geophys. Res., 94, 6995, 1989.

Fuselier, S. A., and D. A. Gurnett, Short wavelength ion waves upstream of the Earth's bow shock, J. Geophys. Res., 89, 91, 1984.

Gallagher, D. L., Short-wavelength electrostatic wave in the Earth's magnetosheath, J. Geophys. Res., 90, 1435, 1985.

Gurnett, D. A., W. S. Kurth, J. T. Steinberg, P. M. Banks, R. I. Bush, and W. J. Raitt, Whistler-mode radiation from the Spacelab 2 electron beam, Geophys. Res. Lett., 13, 225, 1986.

Gurnett, D. A., W. S. Kurth, J. T. Steinberg and S. D. Shawhan, Plasma wave turbulence around the shuttle: Results from the Spacelab 2 flight, Geophys. Res. Lett., 15, 760, 1988.

Hwang, Y. S., and H. Okuda, Low-frequency electrostatic instabilities excited by injections of an electron beam in space, J. Geophys. Res., 94, 10103, 1989.

Kindel, J. M., and C. F. Kennel, Topside current instabilities, J. Geophys. Res., 76, 3055, 1971.

Kurth, W. S., and L. A. Frank, The Spacelab-2 Plasma Diagnostics Package, J. Spacecr. Rockets, 27, 70, 1990.

Miyamoto, K., Plasma Physics for Nuclear Fusion, The MIT Press, Cambridge, Massachusetts, 1989.

Murphy, G. B., D. L. Reasoner, A. Tribble, N. D'Angelo, J. S. Pickett, and W. S. Kurth, The plasma wake of the shuttle orbiter, J. Geophys. Res., 94, 6866, 1989.

Narcisi, R., E. Trzcinski, G. Federico, L. Wlodyka, and D. Delorey, The gaseous and plasma environment around the space shuttle, AIAA Pap., 83, 2659, 1983.

Neubert, T., W. W. L. Taylor, L. R. O. Storey, N. Kawashima, W. T. Roberts, D. L. Reasoner, P. M. Banks, D. A. Gurnett, R. L. Williams, and J. L. Burch, Waves generated during electron beam emissions from the space shuttle, J. Geophys. Res., 91, 11321, 1986.

Nishikawa, K.-I., and I. H. Cairns, Simulation of the nonlinear evolution of plasma waves, J. Geophys. Res., 96, 19343, 1991.

Okuda, H., and M. Ashour-Abdalla, Ion acoustic instabilities excited by injection of a electron beam in space, J. Geophys. Res., 93, 2011, 1988.

Okuda, H., and M. Ashour-Abdalla, Propagation of a nonrelativistic electron beam in three dimensions, J. Geophys. Res., 95, 2389, 1990.

Okuda, H., R. Horton, and M. Ono, Propagation of a nonrelativistic electron beam in a plasma in a magnetic field, Phys. Fluids, 30, 200, 1987.

Papadopoulos, K. D., On the shuttle glow (the plasma alternative), Radio Sci., 19, 572, 1984.

Pickett, J. S., N. D'Angelo, and W. S. Kurth, Plasma density fluctuations observed during space shuttle orbiter water releases, J. Geophys. Res., 94, 3721, 1989.

Prichett, P. L., Spatial coherence during pulsed injection of electron beams, J. Geophys. Res., 94, 12081, 1989.

Reasoner, D. S. D. Shawhan, and G. B. Murphy, Plasma Diagnostics Package measurements of ionospheric ions and shuttle-induced perturbations, J. Geophys. Res., 91, 14699, 1986.

Reeves, G. D., P. M. Banks, T. Neubert, R. I. Bush, P. R. Williamson, A. C. Frazer-Smith, D. A. Gurnett, and W. J. Raitt, VLF wave emissions by pulsed and DC electron beams in space, 1. Spacelab 2 observations, J. Geophys. Res., 93, 14699, 1988.

Reeves, G. D., P. M. Banks, T. Neubert, K. J. Harker, and D. A. Gurnett, VLF wave emissions by pulsed and DC electron beams in Space, 2. analysis of Spacelab 2 results, J. Geophys. Res., 95, 6505, 1990.

Rivas, D. R. and D. E. Hastings, Theoretical interpretation of the electrostatic noise in the space shuttle induced plasma environment, J. Geophys. Res., 97, 17097, 1992.

Shawhan, S. D., Description of the Plasma Diagnostics Package (PDP) for the OSS-1 shuttle mission and JSC chamber test in conjunction with the Fast Pulse Electron Gun (FPEG), Artificial Particle Beams in Space Plasma Studies, Edited by B. Grandel, P. 419, Plenum, New York, 1982.

Shawhan, S. D., G. B. Murphy, and J. S. Pickett, Plasma Diagnostics Package initial assessment of the shuttle orbiter plasma environment, J. Spacecraft and Rockets, 21, 392, 1984.

Siskind, D. E., W. J. Raitt, P. M. Banks, and P. R. Williamson, Interactions between the orbiting space shuttle and the ionosphere, <u>Planet. Space Sci.</u>, <u>32</u>, 881, 1984.

Temerin, M., Doppler shift effects on double-probe measured electric field power spectra, <u>J. Geophys. Res.</u>, <u>84</u>, 5929, 1979.

Tribble, A. C., J. S. Pickett, N. D'Angelo, and G. B. Murphy, Plasma density, temperature, and turbulence in the wake of the shuttle orbiter, <u>Planet. Space Sci.</u>, <u>37</u>, 1001, 1989.

Winckler, J. R., The application of artificial electron beams to magnetospheric research, Rev. <u>Geophys. Space Phys.</u>, <u>18</u>, 659, 1980.

Winglee, R. M., and P. L. Prichett, Comparative study of cross-field and field-aligned electron beams in active experiment, <u>J. Geophys. Res.</u>, <u>93</u>, 5823, 1988.